Master's Thesis

Development of an on-chip model for cardiac arrhythmia and pacing

Investigation of the effect of electrical stimulation and structural patterning on the propagating cardiac action potential and development of analysis tools

June, 2013

Author:
Emelie Leht

Supervisors:
Dries Braeken,
Liesbeth Micholt

LUNDS UNIVERSITET
Lunds Tekniska Högskola

Faculty of Engineering, LTH
Department of Measurement
Technology and Industrial Electrical
Engineering
Division of Electrical Measurements

Interuniversity Microelectronics
Centre, Belgium
Cell and Tissue Technologies

Abstract

Cardiovascular diseases are accountable for almost 50 % of the mortality number in Europe which is why research on its causes is highly prioritised. For practical and ethical reasons, *in vitro* study models are of high importance to enable research on cardiac abnormal behaviours.

To meet this issue, researchers from Imec, Belgium, developed Neuray-II, the second generation of a biocompatible chip with micrometer sized electrodes as a platform for *in vitro* studies of cardiac arrhythmia and pacing. For this study, an HL-1 cell line was used and their action potential waves were visualised with fluorescent imaging. Low and high frequency protocols were applied to perform electrical stimulation with the chip-electrodes to induce pacing and blocking, respectively, of the action potentials. Macroscopic image analysis of time-lapses capturing the stimulation, with a custom developed Matlab-script, did not show any large scale change in action potential propagation, induction, or termination of re-entrant spirals. The local effect of stimulation on a cellular level was analysed with another script developed for this purpose. The single-cell analysis showed that cells were stimulated only in the near vicinity of the selected electrode. The results from the frequency analysis of the cellular signals did not prove that pacing could be performed. In the future, the analysis method needs higher accuracy to provide a valid conclusion. Analysis of the cellular signals from high frequency protocols indicate that local blocking of action might be possible but also needs further experiments for confirmation. Attempts were also made to alter the propagation of action potential waves by structural patterning. This was done by microcontact printing and application of a silicone insert, both with a non successful outcome.

In conclusion the Neuray-II could possibly be used as an *in vitro* model for studies of cardiac arrhythmia and pacing since the basic tools and knowledge have been provided with this project. Further development is needed for completion of a functional model.

Contents

Preface

Firstly, I give my greatest thanks to my mentor, Liesbeth Micholt, who has patiently introduced me to the *in vitro* working procedures, answered many question and been a big support during the process from experimental design to report finalisation. Secondly I give just as many thanks to my supervisor, Dries Braeken, who allowed me into this project to start with and then always kept pushing and wanted me to explore new possibilities and solutions and provided a lot of creativity. I also want to thank Olga Krylychkina for teaching me everything of how to culture cells and take good care of them. Many thanks also to Luis Hoffman for spending time to help me troubleshoot the electrical equipment and also putting me on the right track during software development. A final thank you to everybody included in the Imec, Cell and Tissue Technologies – group to who made me feel very welcome

Last but not least I also want to thank my professor, Lars Wallman, who provided me with the opportunity to perform my thesis work with his department and for the support offered along the way.

List of abbreviations

ADC	analogue-to-digital conversion
AF	activation frequency
AM	acetoxymetylester
APD	action potential duration
bpm	beats per minute
CCD	charged-couple-device
CMOS	complementary metal-oxide-semiconductor
DIV	days *in vitro*
FET	field effect transistor
FITC	fluorescein-labelled isothiocynate
HCN	hyperpolarizing-activated, cyclic nucleotide-gated channels
IC	integrated circuitry
IPI	inter-peak-interval
MEA	microelectrode array
MHC	myocin heavy chain
MUX	multiplexer
NaN	not-a-number
NCX	Na^+/Ca^{2+} exchange
NR ROI	noise reference ROI
PCB	printed circuit board
PDMS	polydimethyl siloxane
POS	point of stimulation
ROI	region of interest
SA node	sinoatrial node
SR ROI	signal reference ROI

1   Introduction – The beat of life

Since ages, our beating heart has been seen as a symbol of life. Each beat pumps fresh oxygenated blood out to our body parts, enabling them to function and allowing us to have an active life. We are dependant of this beat to be autonomous and self-adaptive to our body's level of activity and metabolism. It is when this system seizes to function properly that we encounter issues like heart-failure, heart-attack, arrhythmia and fibrillation, which are all associated with the heart beat rhythm deviating from its normal behaviour. Many of these conditions are life threatening and have become more common with an ageing population.

Studying the mechanisms behind the heart beats, its automaticity, adaptation ability and causes of arrhythmia has therefore become of high interest to prevent the high number of casualties induced by failures. Scientific research in parallel with technical development has so far resulted in tools as the cardiac pacemaker already developed during the 1950's, and the implantable defibrillator introduced during the 1990's [1]. However, cardiovascular diseases are still accountable for up to 47% of the mortality number in Europe [2], which indicates that there is still a lot of research and development needed in this field.

Ideally, research would be performed *in vivo* on a human heart to achieve the most accurate environment. For ethical and safety reasons this is obviously not possible and therefore one need to resort to model systems like animal *in vivo* testing. However, these types of experiments are also surrounded by many ethical restrictions, the use of animals is expensive, animal handling and experiment preparation is time consuming and in many cases the results require a complex analysis system rendering results that can be difficult to interpret due to the many parameters that play a role. For these reasons an approach with 2D tissue cultures *in vitro* is usable for many types of experiments. There are two main types of *in vitro* cultures, being either primary cells or cells from a cell line. Primary cells are extracted directly from an animal, a cell line on the other hand consists of immortalized cells which continuously divide due to their tumour origin. The *in vitro* cell line culture introduces a number of advantages such as: (i) higher flexibility in planning and performing experiments since the aging factor of the animals is eliminated, (ii) cell cultures are kept in small dishes and can be maintained in an incubator system which eliminates the need for a special animal facility, and finally by scaling down the model system a

reduced complexity in analysis can be achieved. An *in vitro* approach also gives the possibility to examine how individual cells reacts in a foreign environment by studying its coexistence with different types of substrates, structures and even electrodes. The latter is of especially high interest for cardiac cells, i.e. cardiomyocytes, due to their inherent electrical activity. The use of electrically active devices, as complementary metal-oxide-semiconductor (CMOS) chips or microelectrode arrays (MEAs), opens up possibilities to both record these electric signals and generate electrical stimuli that can induce and change activity in the cell population. Knowledge gathered from these types of experiments can deepen the comprehension of the parameters affecting the origin of arrhythmia and thereby also give directions on which parameters that should be the target for a termination of the arrhythmia.

At Imec, Interuniversity microelectronics centre, a bio-compatible chip for *in vitro* studies has been developed [3]. The characteristic feature for this chip is its electrode dimension which stretches down to the micrometer scale, and therefore gives the opportunity to perform extremely localized recording and stimulation. This chip, called Neuray-II, is used in research for a number of different applications such as recording of electrophysiological cell signals, performing electroporation and measurements of intracellular potential with extra cellular electrodes [3].

1.1 Aim and outline

The aim of this thesis is to examine whether the Neuray-II chip can be used as a study platform for *in vitro* studies of arrhythmia and re-entry phenomena. To this extent, this needs to be re-created in a 2D tissue culture, similar to what occurs *in vivo* in heart tissue. To accomplish this, firstly the goal is to investigate the effect of highly localized stimulation on the pace of the cells on population level. Answering this question will help us to understand if pacing one cell can affect the pace over the full cell population.

Secondly, we want to investigate if it is possible to alter the pattern of the propagating action potential waves present in atrial cell tissue cultures, or even to terminate the wave propagation by localized electrical stimulation.

Thirdly, to examine whether a more structural cell growth could increase the appearance of re-entry phenomena, two structural patterning techniques are investigated. The methods are based on structural cell growth by micro-contact printing and structural cell-growth around a patterned silicon insert placed in the culture.

The structure of this thesis is outlined as follows:

Chapter 1 is the introduction to the topic together with its aim and the outline.

Chapter 2 first gives the literature overview and an introduction to heart electrophysiology, the cellular mechanisms behind pacing and arrhythmias, an overview of the state of art on how arrhythmia is modelled *in vitro* and a description of the HL-1 cell line used in this research. The chapter also includes basic mechanisms of electrical stimulation and recording of cellular signals, an overview of CMOS and MEA technologies used for this type of experiment and finally a presentation of the Neuray-II chip and its properties.

Materials and methods is the following part, chapter 3, and presents the execution of the experiments and development of the analysis.

Experimental results are described in chapter 4

In the Analysis and Discussion, chapter 5, the results are evaluated and put into a context of the literature background to determine their relevance and applicability for the field.

Finally conclusions and perspectives for future research in this field are discussed in chapter 6.

2 Literature background

To be able to model a malfunctioning heart one first needs to understand the mechanisms of a healthy one. Therefore, the mechanisms for a normal and functional heart cell will be presented in the first paragraphs, followed by physiological explanation of some of the pacing-related diseases mentioned in the introduction which are the target of the study-model. To bring us closer to a functional *in vitro*-model, an overview of methods to induce arrhythmia is presented, followed by the introduction of the cell line HL-1 used in the experiments along with methods used for visualizing arrhythmia. The second part of this chapter introduces the electrical recording and stimulation systems used for cellular signal measurements. The section includes the basics of cellular recording and stimulation, possibilities with CMOS and MEA technology in the field of electrophysiological studies of electrogenic cells and is finished by an introduction to the Neuray-II chip and its features.

2.1 The cardiac cell and its mechanisms – what makes them beat?

2.1.1 Action potentials occurs by ions flowing

Cardiomyocytes elicit intrinsic contraction behaviour coinciding with an electrical signal. This behaviour arises from ion currents flowing across the cell membrane, thereby changing the intracellular fluid to become either more negatively or positively charged. These currents constitute the cardiac action potential. A schematic of the cardiac potential and its most important ionic currents are displayed in Figure 1.
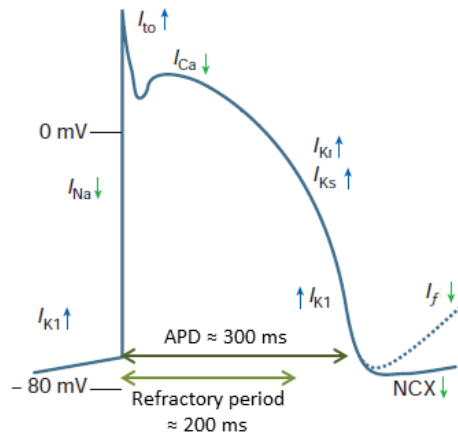
Figure 1: The cardiac action potential. The most important ion currents constituting the action potential. Upwards arrows shows currents going out of the cell, downwards currents going into the cell. The I_K current consists of a rapid and slow part rendering I_{Kr} and I_{Ks}. The full, average action potential duration is 300 ms and refractory period ends at 90% of repolarization. In the figure, the effect of the 'funny' current I_f is also displayed. Adapted from [4].

In Figure 1, four different phases of the action potential can be distinguished. The first and the last phase are resting stages, the second is the 'firing' phase and the third is a 'plateau' phase. The cardiac cell has a resting potential between -70 and -80 mV which is set by the I_{K1} current which lets K^+ ions flow out from the cell. The inwards Na^+ current, I_{Na}, depolarizes the cell and when a threshold is reached the cell will 'fire' the action potential. This is what causes the sharp top in the action potential, see Figure1. When reached its top at around 40 mV the potential will decrease because of repolarization by an outwards K^+ current, I_{to}. The firing phase is followed by the plateau phase in the potential, sustained by the inwards, depolarizing Ca^{2+} current, I_{Ca} [4]. During this plateau state, which is seen as the big bump in the action potential in Figure 1, the entry of Ca^{2+} will trigger release of sarcoplasmic Ca^{2+} which together elevates the intracellular $[Ca^{2+}]$. This enables the binding of Ca^{2+} ions to the myofilaments in the cell thereby activating their contraction [5]. The plateau is followed by outwards K^+ currents, I_K, called the delayed rectifiers, that repolarizes the cell towards its base level of -80 mV. In the last phase of the repolarization the cell is actually slightly depolarized by the Na^+/Ca^{2+} exchange (NCX) which creates an; overall inward current by switching 3 Na^+ for every Ca^{2+} [4]. During this calcium extrusion the intracellular $[Ca^{2+}]$ is naturally decreased which also activates an unbinding of Ca^{2+} from the myofilaments that in turn releases contraction [5]. The time between maximum intracellular voltage and 90% repolarization is reached is considered as the action potential duration (APD) [6]. The cells

refractory period, during which the cell is unable to fire a new action potential, lasts from depolarisation until half of the repolarization phase which is around 200 ms [7]. The APD and the refractory period are also displayed in Figure 1.

2.1.2   The 'funny' current

The origin of the automaticity for spontaneously generated action potentials has been somewhat harder to determine. However, many signs point towards the "funny" current, I_f, as a crucial component for the act of pacemaking [8, 9]. The I_f current is a depolarizing current that has been located to a very specific type of ion-channels named Hyperpolarizing-activated, Cyclic Nucleotide-gated channels (HCN). From the name one can tell that these channels are activated by hyperpolarization, and in the case of cardiomyocytes this occurs after the repolarization by the delayed rectifier currents. The HCN channels will activate a slow inwards current of Na^+ and K^+ and depolarize the cell towards the firing-threshold [10]. An example of where in the action potential the "funny" current occurs can be seen in Figure 1.

The I_f current is present in all type of cardiomyocytes, however not all cardiac regions shows signs of automaticity. This can be explained by the difference in voltage dependence for the HCN channels in the different cell types [11]. The cells that shows the strongest dependence on the I_f current are the cells in the sinoatrial node (SA node), which is found in the right atrium wall in all mammals. These cells are called the primary pacemaker cells. Their spontaneously generated action potentials spread through the heart via the atria, the atrioventricular node (AV node) and the ventricles making the heart contract accordingly [9]. An illustration of the heart and the action potentials appearances from different areas of the heart can be seen in Figure 2. Here one can clearly see how the I_f current has the most depolarizing effect on cells from the SA node.

2.1.3   Spreading the action potential

The conduction of action potentials is enabled by the cardiac myocyte gap-junction which is a connection between the cardiac cells that transmit electrical signals. Gap junctions are formed by a type of ion-channels called connexins. There are several types of connexins which are named after the length of their transmembrane protein and they all differ somewhat in conductance, voltage dependence, pH dependence and ion permeability. When cardiac cells are in close proximity, these channels constitute a direct connection between the cells, enabling the transmission of a depolarizing current and thereby create a conduction path through the cardiac tissue [12].

2.2 Cardiac arrhythmia

A normal, functioning, healthy heart has a regular beating-frequency which is adapted to the body's metabolism and the action potential travels from the SA node like uniform wave through the heart without any disturbances, see Figure 2. However, a number of parameters can affect the sensitive electrical conduction and its path and thereby cause a diversion from the normal functionality.
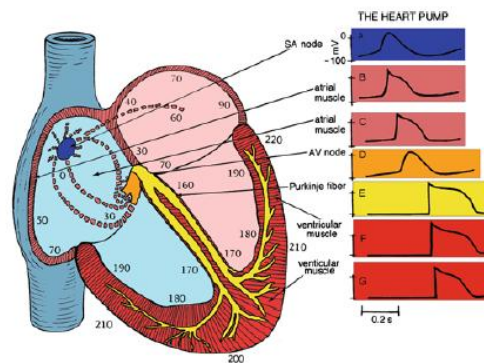
Figure 2. Electrical conduction in the heart. Caption of the heart and the order of the conductional pathway. Normally the action potential origins in the SA-node, propagates via both atria and through the atrioventricular node, passes the bundle of His and then continues via the Purkinje fibre system from which it reaches the ventricular muscle. The appearance of the action potential is displayed for every part of the system, their position on the time scale indicates the activation time relative to the pacemaking signal in the SA-node. Adapted from [13].

Cardiac dysrhythmia or arrhythmia is the collective term used when the heart shows abnormal electrical activity. This includes frequency related phenomena such as tachycardia and bradycardia-when the heart beats too fast or too slow-, and mechanism-related abnormalities as fibrillation, re-entry and automaticity changes. The main focus on this part lies within understanding the origin and features of some of the mechanism-related abnormalities.

2.2.1 Interruption of automaticity

As mentioned earlier, the main pacemaker cells are found in the SA node and their automaticity is believed to be driven by the "funny current" I_f. However, there are a few other regions in the heart that also exhibit spontaneous firing of action potentials, one of them is the His-Purkinje system. The location of this system can be seen in Figure 2. The system constitutes the His-bundle, located

14

between the atria and the ventricles, and the Purkinje-fibres, found in the ventricles, which together are responsible for the fast conduction of the action potential originating in the SA node. The intrinsic firing-rate for the His-Purkinje system is 15-40 beats per minute (bpm), which is much slower in comparison to the SA node that fires 60-100 bpm. Hence, the His-Purkinje automaticity will be overruled in normal case and the system can be seen as a back-up in case the SA node firing fails, making it classified as a secondary pacemaker system [14]. Nevertheless, by having this sort of automaticity present in more than one region, interruptions in the conductivity path can occur if the secondary pacemaking system suddenly starts to fire at a faster rate than intended.

This type of phenomenon is named *triggered activity* and it occurs if a syncope is initiated by the intrinsic automaticity and the propagated action potential. This can result in tachycardia and change of site of impulse originating elsewhere than in the SA node [15]. When the main pacemaker location differs from SA node this is called an ectopic focus [4].

2.2.2 Fibrillation

Fibrillation can occur both in the atria and in the ventricle and is characterized by presenting extremely rapid and irregular activation, 400-600 bpm. This makes it impossible to maintain a uniform excitation of the heart. Instead, one or several ectopic foci will occur producing multiple wavelet pattern or re-entrant spirals [15, 4]. These abnormal, rapid wave patterns can result in a number of pathological and potentially dangerous diseases such as mitral valve disease, congenital heart disease and congestive heart failure for atrial fibrillation [4] and myocardial ischaemia and infarction for ventricular fibrillation [15].

There are two mechanisms through which fibrillation can occur. One possibility is the appearance of a re-entrant circuit due to depolarization by ectopic foci, causing syncopating of the beat to a faster pace. This will be discussed in detail in section 2.2.3. Another possibility is that an "afterdepolarization" occurs, related to the NCX current, described in section 2.1.1. The net of the NCX current is causing an inward, depolarizing current. If the intracellular $[Ca^{2+}]$ is very high or if the activity of the NCX channels are elevated for some reason this can raise the intracellular potential over its firing threshold and cause ectopic firing leading to fibrillation [4].

2.2.3 Re-entry

A re-entrant circuit is classified as a conduction-related abnormality that can lead to arrhythmia. This differs from the mechanisms mentioned above which are rather due to abnormal impulse generation [16]. Hence, the crucial features of re-entry originates in the structure of the myocytes and their conductional ability. Under normal circumstances, the conduction of the action potential through the cardiac tissue is supposed to be unidirectional, along the direction of the myocytes. However, if cells are organized in a loop-structure either due to normal anatomical features or because of scarring, a re-entrant circuit can be enabled. The basic mechanism of a re-entrant circuit in a loop-like structure can be seen in Figure 3.
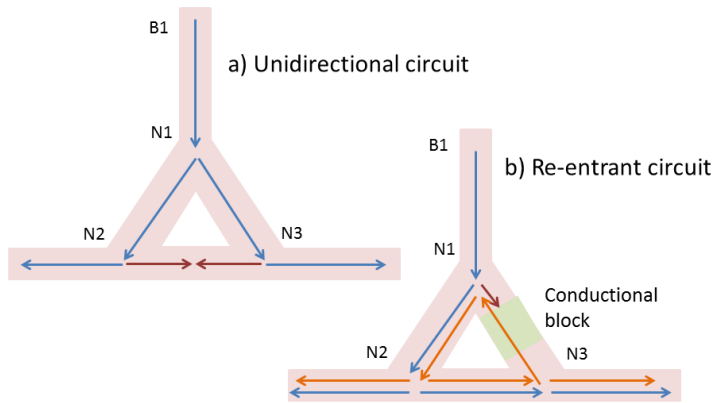
Figure 3. Re-entrant circuit from conductional block. Propagation of action potential (AP) in a loop-like structure indicated by arrows. Blue arrows symbolize normal propagation, red blocked propagation and orange propagation due to a re-entrant circuit. **a)** caption of a normal unidirectional propagation of AP where signal is spread through both nodes 2 and 3 and further on to the sides. Underneath the loop the signal blocks itself since propagation speed is higher than the refractory period. **b)** A block of the propagating AP in the right node enables propagation underneath the node that induces a re-entrant circuit (orange arrows).

Allessie and co-workers modelled the re-entrant circuit mechanism already in 1977 under the name of 'The leading circle model' which still serves as a fundamental explanation of the phenomena [17]. The important parameters of their model are the length of the pathway, L, the conduction velocity, C, and the refractory period, R. The model states that if the dimension of the loop in circumference (L) is equal to or larger than the refractory period times the conduction velocity, $L \geq CR$, a circuit that excites itself, a re-entrant circuit can occur. An example of this event can be seen in a three-node loop-structure in Figure 3. In the normal case, Figure 3 a), the action potential travels from the

top, branch 1 (B1), divides at node 1(N1) to propagate through branch 2 and 3 (B2 and B3) to arrive at node 2 and 3 (N2, N3) at the same time. A loop circulation of the action potential is not possible since the bottom of the loop still is reached by the propagated action potential from two directions at the same time. Propagation is thereby terminated since the neighbouring cells are in their refractory period. However, if one of the branches in the loop is blocked, Figure 3 b), the action potential travels only through the free branch. When the action potential reaches node 2 it can now propagate under the loop and back up through node 3 towards node 1. At this point, if the conditions are fulfilled so that $L \geq CR$ is valid, where L in this case is the path around the loop and R the refractory period of the cells in node 1, a re-entrant circuit can be established that fires itself independent of input from branch 1.

Depending on the mentioned parameters one can understand that when conditions are right, a region firing at a self-sustained, rapid pace can put the cardiac conduction completely out of balance. These three parameters are also the key to how to affect a re-entrant circuit and one can alter the pathway, conduction velocity and the refractory period with different methods.

One of the more pronounced re-entrant circuits that has been the basis for a number of studies is the re-entrant spiral. The re-entrant spiral appears as an action potential-wave that, instead of propagating across the tissue, circles around a node or a loop like structure as the one seen in Figure 3, thereby creating a spiral-like appearance. This type of spirals will be described further in section 2.3.1.2.

Re-entrant mechanisms have turned out to be relevant in a number of tachycardia conditions, and both atrial and ventricular fibrillation [15, 4, 18, 19].

2.3   Towards an *in vitro* model

By having the basics on cardiac cellular function and malfunction one can now explore the possibilities of how to create *in vitro* study-models of cardiac arrhythmias to achieve deeper knowledge about their fundamental mechanisms. Firstly, potential methods on how to induce and terminate arrhythmia are reviewed. This is followed by an introduction to the cell line HL-1 and finally a short overview of how to visualize arrhythmia *in vitro*.

2.3.1   Inducing and terminating arrhythmia

The main goal of the studies of cardiac arrhythmia is naturally to contribute in the development of a successful treatment to terminate arrhythmia. However, to

be able to study arrhythmia termination one also needs to be able to induce it, therefore both topics are of high interest. Further on, by studying and modelling the induction of arrhythmia more precise knowledge can be gathered on its mechanisms, which in turn facilitates the understanding for its termination. The three main methods used for these types of studies are drugs, electrical stimulation and structural patterning which all target different features.

2.3.1.1 Drugs

Antiarrhythmic drug treatments have been used for quite some time and their - in many cases- coexisting proarrhythmic effect has been known for some decades. The last 25 years it has been acknowledged that antiarrhythmic drugs rather increases risk of tachycardia and fibrillation due to occurrence of re-entry. The increase of re-entrant circuits is due to mechanisms such as the decrease in conduction velocity by the pharmacological block of different types of ion channels. However, the *in vitro* approach is widely used as a platform for screening of new drugs to determine if they possess proarrhythmic effects or not.

2.3.1.2 Spontaneous induction

Not very surprisingly, it has been shown that re-entrant spiral waves in cardiac cell cultures can occur spontaneously without any addition of drug or electrical stimulation [20, 21, 22]. When the spirals emerge depends somewhat on plating density and type of cells but if they emerge spontaneously they usually do so around the third day in culture. The spirals' features as rotation and conduction velocity also increase with time in culture [21, 22]. This type of spontaneously occurring re-entrant spirals might not be controllable to an extent wanted for a study model, and re-entrant spirals do not always occur spontaneously in which case one need to induce them manually.

2.3.1.3 Electrical stimulation

Due to the many complications in pharmacological arrhythmia treatment, alternative methods for affecting arrhythmias have been explored for quite some time. Since the threshold for cardiac action potential firing is regulated by a voltage change, it is therefore susceptible to electrical stimulation. This feature has proven to be a far better target for activation and deactivation of action potentials and their properties, since it operates on a voltage-basis rather than blocking of specific channels, like pharmacological treatments do.

Briefly, the mechanism of electrical simulation functions as follows. In resting state, there is a potential gradient over the cellular membrane rising from the highly negatively charged intracellular environment and the positively

charged extracellular fluids. When an electrode is placed extracellular and adjacent to the cell it will alter the membrane potential. A cathode will shift the membrane potential so the inside of the cell becomes more positive, thereby depolarizing it. If the shift is big enough, depolarization will reach the firing threshold and an action potential is generated. If the electrode is an anode the potential shift will instead hyperpolarize the cell. It is also possible to insert an electrode intracellular and eject current into the cell which will change the membrane potential accordingly [23, 1].

There is a vast number of successful trials of inducing different types of arrhythmia *in vitro*. This subsection will be restricted to a brief overview of some of the studies where pacing and/or re-entrant arrhythmias could be induced and the methods used.

A) Unipolar electrode stimulation

Several cases of induction of re-entrant spirals by electrical stimulation have been shown by using either field stimulation, stimulation by a unipolar electrode or both. The unipolar electrode stimulation seems to be preferred in more complex studies where the combinational effect of re-entry and a secondary feature is investigated. Secondary features investigated so far are altered spatial structure, types of ion channel blockers and other pharmacological substances with possible effect on the currents involved in the action potential [24, 25, 26, 27]. The advantage is that the point electrode stimulation highly resembles an ectopic focus and induces a very local stimulation which later can spread through the cardiac network as a non-artificial signal. The general method for inducing this type of re-entry is to stimulate the culture by a period of pacing to a slightly higher frequency then the one intrinsic for the culture, 1 - 10 Hz is commonly used.

B) Field electrode stimulation

The field induced stimulation is less common for induction of re-entry since it targets a larger field for excitation. Since re-entrant circuits usually occur around small dimension obstacles and conduction loops, stimulation by an electric field is not very effective since it does not deliver the local conduction disturbance needed for a re-entrant circuit to emerge. Nevertheless it is possible to induce pacing this way, as proven by Brundel and co-workers 2004, who managed to induce pacing and tachycardia *in vitro* to investigate whether activation of the protease calpain is crucial for Ca^{2+} current alteration that is observed during atrial fibrillation [28]. Commercial instruments for this type of *in vitro* pacing have since been developed and successfully used [29].

One of the studies which has showed the most controlled induction of re-entry used a combination of both field and unipolar electrodes. The protocol for induction uses pulsed field stimulation to first activate the whole culture followed by point stimulation for induction of re-entry [30].

C) Blocking of action potentials and re-entrant arrhythmia

Electrical stimulation can not only be used for induction of pace and arrhythmia but also for blocking action potentials and termination of arrhythmia. The methodology for this is to aim for a saturation of the intracellular potential and thereby to prevent firing of new action potentials. The type of stimulation required to achieve this state is therefore of a higher magnitude and/or frequency than for pacing and arrhythmia induction.

Dura and co-workers made a study on HL-1 cells (described further in section 2.3.2) grown on a MEA. The MEA was used for both pacing the culture and blocking of the propagating action potential waves by applying high frequency stimulation. This type of blocking enabled complete screening of areas so that no action potential waves could pass the electrode and one also managed to change the direction of propagating waves by blocking certain areas in the propagation path [25].

Termination of re-entrant arrhythmias by stimulation has also been accomplished *in vitro*. Iravanian and co-workers made use of their combinatorial stimuli mentioned above and by creating a signal of both field and single point stimulation they could terminate the re-entry spirals that they had induced in a controllable manner [30].

2.3.1.4 Patterning

As mentioned in the Re-entry subsection, section 2.2.3, physiological obstacles in the tissue can act as cues for re-entrant circuits and the morphological structure of the heart and its arrangement of cells is to a large extent responsible for its conductional features. In an *in vitro* tissue culture one loses several spatial cues for cell growth that would induce a more ordered cell structure. Some attempts to mimic spatial cues and thereby affect *in vitro* culture features are presented in the following paragraphs.

The use of co-cultures is probably the least artificial solution to achieve a more structured cell culture. Chang and co-workers used a rat ventricular myocyte-human skeletal myocyte co-culture to model an area exposed to infarction. Due

to the presence of skeletal myocytes a higher and more dispersed conduction velocity was achieved and re-entry could be induced [27].

It is also possible to introduce engineered structures to affect the culture. For instance, HL-1 cells were grown on nanometer sized grooves, which were to resemble the structured extra cellular matrix. The cells showed a high degree of alignment with the grooves, a significantly higher conduction velocity than cells on a cover slip and contraction was also aligned with the grooves [26]. The groove-structure, the cells alignment and their anisotropic conduction can be seen in Figure 4 a,b,c). Lim and co-workers also showed how introducing small obstacles as holes in a cover slip can induce anchoring onto those objects by re-entry spirals [31].
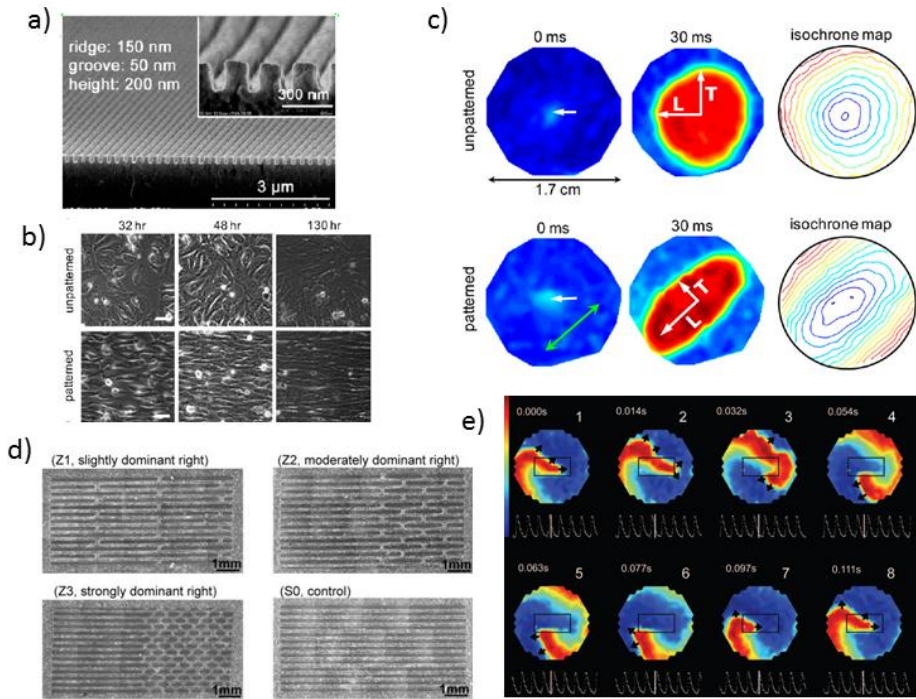
Figure 4. Patterning methods. Captions from the studies by Kim and co-workers [26], a-c) and Bian and co-workers [24], d,e). **a)** Nanometerscaled grooves of hydrogels on glass substrate. **b)** Comparison of cell growth directionality for patterned and un-patterned surface. **c)** AP-propagation visualized by voltage sensitive dye. Green arrow indicates longitude direction of grooves. **d)** Cells growing on micro-contact printed surface. **e)** Visualization of induced re-entry occurring around printed pattern. The location of the pattern is indicated by the black box.

A third method to arrange a cell culture is by the use of micro-contact printing. Bian and co-workers made use of this technique by making a stamp that patterned the cell culture substrate with the coating normally used to make the cells attach to the substrate. This way a net-like pattern of cells could be induced around which re-entry could occur [24]. The printed pattern and a re-entry caused by it can be found in Figure 4 d,e.

2.3.2 The HL-1 cell line – a well-known substitute for primary cardiac cells

When developing an *in vitro* model, the use of a cell line might be preferable to primary cells since it eliminates the handling of animals and thereby also lower time and costs. The requirement is that the cell line has high enough similarity in its features of interest to the primary target cell to justify its use as a replacement. In this study the cell line HL-1 is used as a replacement for primary atrial cardiac cells.

The HL-1 cell line has been developed by Claycomb and co-workers [32] and they showed that the cell line, derived from a mouse atrial cardiomyocyte tumour linage, can proliferate in culture, can be passaged and that both its differentiated cardiac myocyte phenotype and the contractile activity can be maintained. Some indicators showed for differentiation are presence of expression of adult isoform myocin heavy chain (MHC), which is a contractile protein isoform, expression of α-cardiac actin, which also is found in adult mouse ventricular cells and expression of the protein Connexin43 which is present in the adult gap junction. The HL-1 cell line also showed to have spontaneous action potentials and synchronous beating in confluent cultures [32].

The above mentioned features and further characterisation of the HL-1 cell line proved it to be useful for a variety of *in vitro* model systems which were reviewed by White and co-workers [33]. Considering electrophysiological studies targeting cardiac phenomena by *in vitro* modelling, the study by Sartiani and co-workers is of high interest, since it further characterizes several important electrophysiological features of HL-1. The investigation showed presence of the HCN gated channels and their related I_f current, which is believed to be crucial for the pacemaking function. The HL-1 I_f current was characterised to have a high resemblance with the one found in primary cardiac cells in threshold potential, action potential amplitude and conductivity [34].

As a matter of fact, the HL-1 cell line has become a highly favourable replacement for primary cardiac cultures. It has already been mentioned as culture of choice in a few arrhythmia studies in previous subsections but it has also been specially characterized for being suitable for modelling of re-entry spirals [21].

2.3.3 Visualizing arrhythmia

Previous *in vitro* studies, the propagation of cardiac potentials and arrhythmia has mainly been visualized with different optical imaging techniques which are presented below.

2.3.3.1 *Imaging with dyes*

Optical imaging is generally carried out by using fluorescent markers to target the mechanism or feature of interest. The markers of choice for visualizing electrical signals of cells are voltage-sensitive dyes and -especially for cardiac and HL-1 cells- intracellular Ca^{2+} markers. The voltage-sensitive dyes, e.g. di-4-ANEPPS, have a chromophore as an active agent that displays a spectral change with changes in the surrounding electric field [35]. Using this type of dye one can directly visualize the voltage shift occurring during action potential propagation in cultures [36, 37]. However it has also been shown that voltage-sensitive dyes can induce photodynamic damage by affecting the action potentials. Shaffer and co-workers showed an increase in cardiomyocyte APDs during use of di-4-ANEPPS. The effect was believed to be associated with the release of oxidative intermediates [38]. Larsen and co-workers recently showed a decrease in conduction velocity in guinea pig hearts during application of di-4-ANEPPS [39]. APD prolongation can give rise to arrhythmic "afterdepolarizations", described in section 2.2.2 and decreased conduction velocity is connected to introduction of re-entry, 2.2.3. An example of imaging with a voltage sensitive dye can be seen in Figure 5 a).

The intracellular Ca^{2+} marker is rather an indirect marker since it does not visualize change in electrical activity per se. Nevertheless, it is an available option for displaying electrical changes in cardiac and HL-1 cells since inwards and outwards currents and intracellular release of sarcoplasmic Ca^{2+} are major events of the action potential. One commonly used Ca^{2+} marker is Fluo-4, which is an improved version of its precursor Fluo-3 [40, 41]. The function of the Fluo-family of dyes is based on a complex containing a calcium-binding site and a fluorogenic molecule. When Ca^{2+} is bound to the binding-site, the fluorescence increases up to 40 times [41, 42]. The Fluo marker is an intracellular marker and can be loaded into the cytosol bound by an acetoxymetylester (AM). After

entrance in the cell this bond in cleaved by aspecific esterases, avoiding diffusion of the Fluo-4 back outside the cell. The excitation wavelength is in the visible spectra. Argon-lasers (488nm) are commonly used for confocal or multiphoton miscroscopy [42]. The main difference between Fluo-3 and Fluo-4 is an adaptation to better fit the usage of this laser. The Fluo-4 fluorophore is therefore modified to yield a higher absorbance at 488 nm which increases fluorescence [40]. An example of imaging with Fluo-4 can be seen in Figure 5 d).

There is however one main disadvantage of using a dye as a marker, namely the phototoxic effect. Phototoxicity occurs during the intense illumination that is required to excite the fluorophores. The illumination generates reactive radical oxygen that can damage proteins, nucleic acids or the cell membrane. Some factors that affect the phototoxicity are: (i) the wavelength, longer wavelength reduces phototoxicity, (ii) shorter duration and lower power of exposure reduces the damage, (iii) the type of dye, xanthenes and cyanides increases damage, (iv) concentration of dye, where higher concentration increases damage [43, 44].
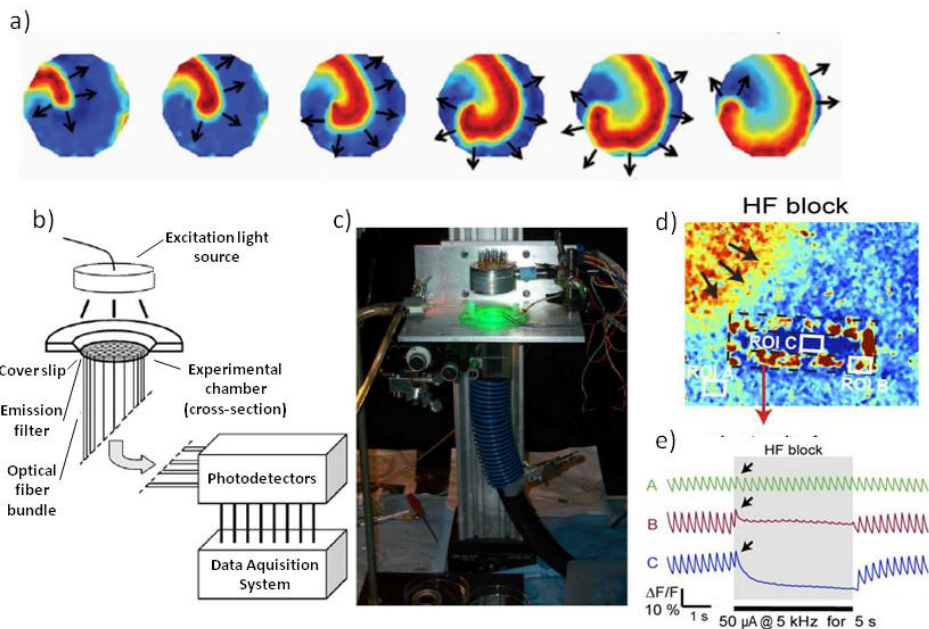
Figure 5. Methods for visualizing arrhythmia. a) Sustained re-entrant spiral captured by Chang and co-workers with fluorescent contact imaging [27]. **b)** Technical illustration and **c)** photograph of fluorescent contact imaging setup developed by Tung and co-workers [45]. **d)** Fluorescent Ca^{2+} imaging and **e)** electrical recording of extracellular signals of a high frequency (HF) block performed by Dura and co-workers [25].

The most straightforward way to image with dyes is using a confocal microscope equipped with the laser of the right excitation wavelength. As mentioned, intense laser illumination can induce phototoxicity. Therefore, the laser scanning time has to be restricted to the minimum. To solve this issue more advanced fluorescent imaging systems have been developed, as the one by Tung and co-workers called *contact fluorescence imaging*. Tung and co-workers uses a voltage-sensitive dye on their sample which was lit by a diode array from the top for excitation. An array of optical fibres underneath the sample transferred the optical signals to an array of photodetectors that enabled simultaneous mapping [45]. A schematic and an image of the contact fluorescence imaging setup can be seen in Figure 5 b,c) and some images captured with this technique in 5 a). Post processing of the recorded signals is required to create the final image of signal propagation and can be done by, for example, implementing cross-correlation scripts to compare the different signals [30]. This method has proven to be very successful and was used in a range of studies [24, 27, 26, 46, 31, 30]. The main drawback with this system is that it requires transparent samples.

2.3.3.2 *Imaging without dyes*

To completely avoid the invasiveness of dyes an imaging technique that captures the contractile motion of cardiac cells has been developed [22]. The method is based on propagation-induced phase contrast imaging which can be realized with a relatively simple setup consisting of a halogen lamp, focusing lenses, a diffuser, a pinhole and a digital camera. Measurements can be carried out continuously for several days and time-difference image processing reveals the propagation patterns with high enough temporal resolution, 200 ms image interval, to visualize spiral pattern on the mm-scale. Also this method has been used for a number of studies of arrhythmia phenomena [22, 21, 20]. The drawbacks of this system are that the spatial resolution is dependent on the camera and, as for contact fluorescence imaging, a transparent substrate is required.

Dura and co-workers have taken a few steps towards visualizing propagation of action potentials by recording with a MEA with a small array of 6 x 6 electrodes that was usable for simultaneous recording [25], see Figure 5. But other than that the field is unexplored at the moment.

2.4 Cells and CMOS – a boost for electrophysiological cell measurements

2.4.1 Background and function

The main drivers for the development of biocompatible CMOS-measurement systems are the urge for understanding the electrophysiological properties of the neuronal signalling system including signalling in the brain, tightly followed by research conduction in cardiac systems, which in many ways show similarities to neuronal networks. To be able to thoroughly map electrical signals in a neuronal network there has been a need for a recording system with a low noise and high spatiotemporal resolution, a specification that has been realized by the fast scaling of CMOS technology and the possibility of producing high density, integrated electronics on a very limited area.

2.4.2 Preceding methods and their limitations

Until the introduction of IC (integrated circuitry) CMOS microelectrode arrays (MEAs), recordings of cellular electrical activity have been restricted to the use of techniques as patch clamp, separately circuited electrode arrays or indirect optical measurements with voltage sensitive or specific ion-targeting dyes, which all have their own advantages and drawbacks [47]. An overview of optical measurements can be found in section 2.3.3.1.

Patch clamp is an intracellular recording method where the membrane of the cell is punctured by a glass pipet in which an electrode enables recording of the voltage or current variations in the cytosol. The method gives a very accurate electrical measurement but is -due to the rupture of the cell membrane- also highly invasive, which limits the duration to short term experiment only. Furthermore, the patching procedure is highly time consuming and not suitable for multiple simultaneous measurements [48, 47].

For extracellular measurements, external metal electrodes and electrode clusters have been the obvious choice. The first generation of MEAs developed during the 1980s was better suited for multi-channels recording than patch clamp by providing up to 64 recording sites. However, no signal could be processed on chip, which required separate circuitry to every electrode which only enabled sequential scanning and also induced parasitic capacitances limiting the signal transduction [49, 47].

2.4.3 The introduction of IC and CMOS

When fabrication of MEAs based on integrated circuitry platforms commenced, this enabled a technological leap for the signal processing and data handling because of the possibility to perform a number of important on-chip signal operations. Some of the crucial integrated components are briefly described here.

Firstly, the multiplexer (MUX), a signal selector, can switch between incoming data lines and forward one of them as an output. The implementation of this component facilitated the development of individually addressable electrodes and also enabled an increase of maximum number of addressable electrodes. Secondly, on-chip amplification for each electrode enables recording of small signals with smaller electrodes. The smaller the electrode size, the higher spatial resolution that is provided. Thirdly, Analogue-to-digital conversion (ADC) can also be realised by IC technology and enables the recorded analogue signal to be converted to digital data, which is easier and faster to process [47, 49].

Finally, by the introduction of IC CMOS technology one also gets access to the usage of field effect transistors (FETs) as the sensing element which has the huge advantage of being bidirectional in its performance. Hence, the CMOS FET system can be used for electrical stimulation as well as recording from the same electrode [47].

2.4.4 Basics of recording and stimulation

To facilitate the understanding of the electrical interaction between the sensing element and the cell, an equivalent circuit is usually modelled. Hodgkin and Huxley developed in the 1950s the first equivalent circuit model of an electrogenic cell, a squid neuron in their case, which describes the electrical function of the membrane and its channels [50]. This model has proven to be very successful and is widely used under the name of the Hodgkin-Huxley model. It describes the cell membrane as a capacitance, C_M, the voltage gated channels as tuneable resistors with nonlinear conductances, g_x, where x represents the specific ion, I_x is the specific ion current, g_L and I_L represents the linear currents and their conductance. The voltage sources E_x have their origin in the Nernst potential that occurs due to ion concentration gradients across the membrane [47, 50]. The upper part of Figure 6 shows the equivalent circuit for the cell and displays the channels with its corresponding components. When putting the cell on top of a sensing element, represented by the lower part of Figure 6, additional components in the circuit occur. The gap between the cell and the sensing element is modelled as a resistance, R_{Gap} and the electrode-

electrolyte interface is normally approximated to a resistance in parallel with a capacitor, R_E and C_E. There is also an additional resistance, R_{Seal}, which determinates the ability to spread currents through the extracellular fluid. The complete, general equivalent circuit for the cell membrane and its coupling to the electrode can be seen in Figure 6.
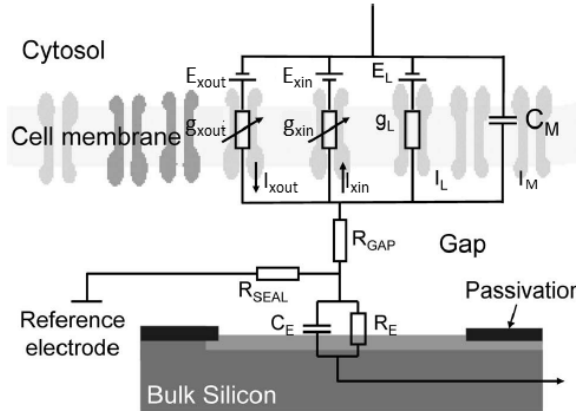
Figure 6. General equivalent circuit for cell membrane and electrode. The voltage gated channels are modelled as tuneable resistors and linear currents are gathered under I_L gated by a constant resistor with conductance g_L. For a cardiac cell the main inward voltage gated current is I_{Na} and to some extent I_{Ca}, a strong outward voltage gated current are the rectifiers I_{Kr} and I_{Ks}. The cell couples to the electrode via a connection affected by gap and sealing resistance and electrode resistance and capacitance is material-dependant. Adapted from [47].

To record a strong signal, the crucial parameters to optimize are (i) the currents, I_x and I_L, (ii) the sealing resistance and (iii) the electrode resistance and (iv) capacitance. The currents will increase with larger cell size due to increased number of ion-channels. The gap resistance is usually small and therefore neglected whilst the sealing resistance should be kept as high as possible to prevent the electric signal from spreading in the medium rather than towards the electrode. As will be seen further on, the sealing resistance can be increased by altering the electrode's spatial structure.

Regarding the electrode parameters, the cutoff frequency is on the order of 1 Hz while cellular signals are on the order of kHz, which means that the electrode will act purely capacitive and not transfer any charge. However, to minimize the delay in the circuit it is still important to keep the electrode resistance low [47].

2.4.5   Electrochemical dynamics of recording and stimulation

A complete model of the electrochemical interaction occurring between the electrode surface and the electrolyte is rather complicated and highly dependent on both electrode material and electrolyte substances. As a very simplified model the recording process can take place as follows. A cell that fires an action potential will redistribute and change the concentration of ions in the electrolyte. This change in ion concentration affects the capacitive element in the electrode, since the accumulation of charges at the electrode/electrolyte interface will change. Subsequently, this can be registered as a change in voltage drop over the capacitor which can be used to determine the strength of the signal [51].

When performing stimulation with the electrode, the mechanism is the opposite. An induced change in voltage over the capacitive element redistributes the accumulated charges on the electrode surface, thereby inducing ionic currents that can depolarize the cell. This process is called charge injection and can be either purely capacitive, i.e. no charges are transferred from electrode to electrolyte or it can be Faradaic which is an oxidative process where an exchange of charges can occur between electrode and electrolyte. The latter process is restricted to stimulation only and does not occur during recording. The Faradaic injection is usually unwanted since the oxidation process changes the composition of the electrolyte which in worst case can introduce toxicity. However, Faradaic injection can be avoided by carefully choosing electrode since this type of injection is determined by the electrode material[52].

As mentioned, the mechanism described above is a very simplified version and the interested reader is directed to consult the Helmholtz plane theory, the Gouy-Chapman theory and the Gouy-Chapman-Stern model for a more detailed description of the electrode/electrolyte interaction [53].

The stimulation and recording mechanisms described in this section are mainly valid for electrical sensing elements as metal electrodes and MOS FETs. However, with the development of more specialized sensing electrodes and FETs such as ion-selective electrodes and ion-selective FETs, enzyme-selective FETs and robust charged-couple-devices (CCDs) it is possible to realize very specialized monitoring systems [54, 55, 56, 57].
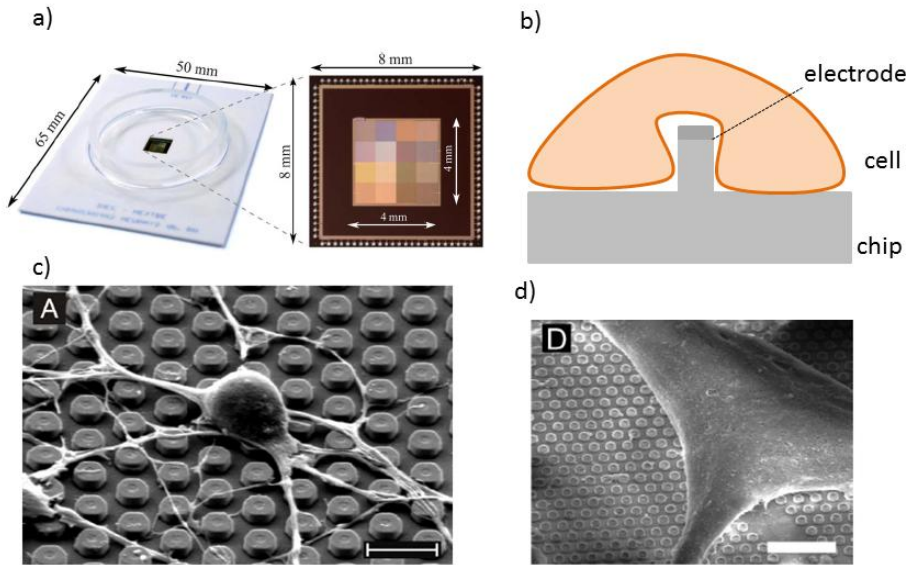
2.4.6 The Neuray-II chip

The Neuray-II chip developed at Imec is, as can be deduced from its name, a second generation chip manufactured for investigation of electrical activity in neurons and neuronal networks. The chip has been realized for a commercial mixed-signal 0.18 μm CMOS-technology with 16 384 electrodes in a varying range of diameters and lengths. All the electrodes are individually addressable and usable for both recording and stimulation [51].

The two main features that define the Neuray-II chip are the electrode's height and diameter.

Due to the electrodes' hexagonal shape, the diameters of the electrodes are rather converted to top areas which have an area of 1.3, 1.7, 2.6, 3.7, 5.1, 6.7, 10.4 and 15.0 μm^2, respectively. Using electrodes on the micrometer-scale allows to have a very high spatial resolution considering that a typical neuron soma is 5 - 135 μm [58]. When the electrode size is equal to or smaller than the cell soma it is possible to perform highly localized and even single-cell recording and stimulation. Figure 7 a) shows the appearance of the chip in its dish and in the magnification of the die where the different areas with different electrode sizes are visible.

The second important feature is the height of the electrodes which are formed as nails. The reason for this is the implementation of the engulfment theory which states that if nail-shaped electrodes are formed of the right material and dimension, cells grown on top can engulf and almost completely surround a single electrode [59]. This engulfment would lead to a better coupling with the cell, giving rise to an increase of the important seal resistance, thereby improving cell-electrode signal transduction both for stimulation and recording. For further investigation on this concept, different heights of electrodes were implemented on the chip [51]. A schematic of engulfment of an electrode by a cell can be seen in Figure 7 b)

Figure 7. Design of the Neuray-II chip. a) Photograph of Neuray-II chip and the die with indicated measurements. On the die the different squares visible are areas with different electrode sizes [60]. **b)** Schematic of how a cell can 'engulf' an electrode. **c)** Scanning electron micrograph (SEM) on a primary hippocampal neuron (3 DIV) on top of the chip electrodes [61].**d)** SEM image of an HL-1 cell on top of the chip electrodes [62].

When the chip was put to experimental use recording on neuronal signals has unfortunately not yet been acquired [51]. However, several successful trials have been made with primary cardiac and HL-1 cultures.

Huys and co-workers performed single-cell, extracellular recordings of primary cardiac cell action potentials with the chip, and verified this with patch clamp measurements. Furthermore, they showed single-cell pacing by stimulation from the electrode and local spreading of the action potential to adjacent cells via gap junctions, also verified by patch clamp [60]. An SEM image of primary hippocampal neurons on the chip electrodes is shown in Figure 7 c).

In trials with HL-1 culture Braeken and co-workers also showed the possibility to induce a state called *open cell* with *Neuray-II,* a mechanism earlier described by Xie and co-workers [63], This condition is reached by high amplitude stimulation with frequencies higher than the cells intrinsic action potential frequency. The stimulation generated transient pores in the cellular membrane and thereby gave access to the intracellular environment. When the open cell state was reached, recordings from the engulfed electrodes were performed.

These recordings showed that the open cell state had given access to the intracellular potential and possibility to measure intracellular signals [62].

Although the chip has proven to be functional for both recording and stimulation, at least for cardiac and HL-1 cultures, there is still one major limitation in the chip design that restricts the usage. Due to the one channel line-out it is not yet possible to simultaneously record or stimulate several electrodes at once which makes it impossible to perform, for example, a matrix recording. It is also not possible to stimulate on one electrode and record on another simultaneously, which is why patch clamp has been used for verification of the stimulation-experiment [62].

3 Material and methods

3.1 Cell culture and sample preparation

The HL-1 cell line was provided by Dr William C. Claycomb (Louisiana State University, Baton Rouge, LA, USA). Until start-up of the culture, the cells were stored in liquid nitrogen. Culturing of the cells was carried out in Claycomb medium (SAFC Biosciences), specially adapted for the HL-1 cell line, with addition of 10% fetal bovine serum, 0.1 mM norepinephrine (Sigma), 2 mM L-glutamine, 100 U/ml penicillin, and 100 mg/ml streptomycin (all from Life Technologies). The medium was refreshed every day except during weekends and a 1/3 split was performed at confluency 2 times/week.

Prior to plating, the chips were rinsed 3 times followed by soaking during 30 min with 70% EtOH. Thereafter chips were rinsed 2 times with autoclaved H_2O (High purity water). Glass coverslips for control samples were soaked in 70% EtOH and quickly flamed. To enable attachment of cells, coating of sample surfaces was done overnight in the incubator with a solution of 5 µg/ml fibronectin in 0.02% gelatin (both from Sigma).

Plating of cells was done at 300 cells/mm^2 or 600 cells/mm^2 to investigate density dependence of the culture. The samples were then kept in an incubator at 37º C with 5% CO_2 for 4 or 5 days until confluency was reached.

3.2 Fluorescent imaging

To ensure a proper distribution of the Fluo-Pluronic mixture over the sample, the cell medium was removed and put into a plastic vial where the Fluo-4 AM in Pluronic (both from Invitrogen), 0.5µg/µl, was loaded to a final concentration of 5 µg/ml in medium and resuspended. The medium was then added to the sample again and was incubated for 30 min. Images and movies were acquired with Zeiss LSM 780 upright confocal microscope using 5x, 10x immersion or 20x immersion objectives. Excitation wavelength used was 488 nm to excite the Fluo-4 and for visualizing the chip surface in reflectance mode. Detection bands were 490-586 nm and 490-604 nm for Fluo-4 and chip surface visualisation respectively.

For the working principles of Fluo-4, see section 2.3.3.1.

3.3 Measurement setup and controller software

The chip was placed in the in-house designed Printed Circuit Board (PCB) – controller which enables computer interfacing via USB 2.0 connection. The measurement setup was mounted on the microscope stage. Customized developed controller software was used to create, load and perform stimulation protocols, recording of cellular electrical signals and impedance measurements.

3.4 Stimulation experiment

3.4.1 General procedure

Prior to stimulation experiment, a general check of the sample was performed to state the general viability of the cells and to ascertain if calcium waves and/or re-entrant spirals were present. Overview images of cells and surface and time lapses of cell-activity were acquired for comparison between cultures and between samples plated with high and low density. Previous in-house experiments showed that the larger diameter electrodes provided the highest voltage stimuli and therefore the stimulation experiments were restricted to those. The choice of the cell selected for stimuli was primarily based on the cell location, ideally directly on top, or in the very close proximity to an electrode. Preferably the cell also showed some intrinsic activity in the fluorescent imaging. If spiral or circular movements were detected in the calcium waves, cells for stimulation were selected close to the centre of the spiral. Time lapse recording was started prior to stimulation to acquire a control period for every recording. Stimulation was initiated via the controller software and when the stimulation output was visualized in the acquisition part on the controller software, the time lapse cycle was noted down. Time lapse duration was adapted so that an image sequence was acquired also after stimulation was stopped. A range of different resolutions was used for the time lapse acquisition to investigate optimal scanning speed versus image size for analysis of single-cell signal recordings and wave pattern recordings.

3.4.2 Stimulation protocols

Stimulation protocols were divided into two sets according to purpose. The first set of protocols contained low-frequency protocols applied for pacing of the cells. Generally, the protocols tested ranged between 1-3 Hz, had an amplitude of 1.65 V, a signal pulse width of 5 ms and a total duration of 30 s. Choices of pacing frequency, pulse width and duration were based on earlier similar trials found in literature [46, 30, 27, 24, 28, 25]. Biphasic pulse stimuli were used since it decreased appearance of Faradaic processes [52] and the amplitude has

been shown to be a good starting amplitude during previous in-house experiments, since it ensured a strong enough stimulation to affect the cell as long as the coupling between cell and electrode was good enough. Trials to test somewhat higher pacing frequencies were also performed and some tests were carried out with lower amplitudes in attempt to detect the required voltage threshold. These protocols were applied 1-2 times per time lapse, and the specifications are summarized in Table 1.

The second set of protocols was made with the aim to block the periodic pacing of the cells and thereby also block spreading of the wave. These protocols were mainly based on an earlier study by Dura and co-workers [25] and frequencies used ranged from 500 Hz - 5 kHz. As earlier, a biphasic pulse with amplitude 1.65 V was used. The pulse width was adapted to be half of the pulse period. The total duration of pulse train ranged between 0.5 – 10 s and the number of pulse trains per time lapse was 2-5. Protocols are summarized in Table 1.

The high frequency (*f*) protocols were applied both as single-electrode experiments and as sequential stimuli where a row of electrodes was stimulated. The sequential stimuli was achieved by manually switching in the software the electrode that was to be stimulated.

Table 1. Stimulation protocols

Low *f* protocols - pacers		High *f* protocols - blockers	
Frequency (Hz)	Amplitude (V)	Frequency (Hz)	Amplitude (V)
1	1.65, 1.5, 1.3, 1, 0.5	500	1.65
2	1.65	1000	1.65
3	1.65	2000	1.65
5	1.65, 1.3, 1.2, 1.1, 1, 0.5	5000	1.65
10	1.65, 1.2, 1		

3.5 Patterning for a structured cell growth

Two methods for introducing structures in the cell culture that potentially could affect wave propagation and occurrence of re-entrant circuits were briefly explored, i.e. microcontact printing and the application of a silicone insert.

3.5.1 Structured growth by micro contact printing

Similar to experiment by Bian and co-workers [24], usage of structured micro contact printing with fibronectin was applied.

3.5.1.1 Stamp fabrication

A polydimethyl siloxane (PDMS) stamp with a grid-like pattern was fabricated as follows.

As a pattern-master, an already existing silicon wafer with an SU-8 pattern was used. The wafer was placed in a holder with a tube on top into which the PDMS was poured. The whole holder was put into a vacuum chamber to degas the PDMS. After, the whole holder was put into an oven at 110 ºC for curing for 1h. When cooled down, the stamp was removed from the holder and wafer.

3.5.1.2 Microcontact printing protocol

To verify pattern functionality and the optimal printing technique a first trial was made with fluorescein-labelled isothiocynate (FITC) in PLL (Poly-L-Lysine) (Sigma), 0.5 mg/µl, as printing agent, EtOH cleaned glass coverslips were used as samples. The stamp pattern was covered with fluorescent PLL 1 min, blow dried with N_2 and then placed upon the coverslip for 1 min. Different placement and pressures were applied to different samples to find the best pattern transfer protocol. The sample was thereafter put in Ethanol amine (ETA) (Sigma) blocker 1 min followed by rinsing 2 times 1min in phosphate-buffered saline (PBS) (Invitrogen).

A solution of 5 µg/ml fibronectin in 0.02% gelatine was eventually used instead of the FITC-PLL to coverslips prepared for cell culture, keeping the rest of the protocol the same. Several pressure and placement techniques were applied to these samples as well.

The placement and pressure methods used were the following:

1. The cover-slip was placed in a clean dish, the coated stamp was carefully placed on top of the cover glass. The stamp was lightly pushed from the top and then released.
2. The cover-slip was placed in a clean dish, the coated stamp was placed on top of the cover-slip and a light constant pressure was maintained for 1 minute.
3. The cover-slip were placed with the tweezers onto the stamp pattern and lightly pushed with the tweezers to attach. The stamp was then placed with the cover slip downwards in the dish as described above. The stamp was given a light push and was then released.

3.5.2   Structured cell growth with a silicone-insert

A grill-like silicon insert constructed by micro-dissecting tools was used to examine the effect of larger structures on the cell culture. The insert was gently dipped into PDMS, placed on the chip and then cured for 1h in 110 ºC prior to plating of cells.

3.5.3   Cell culture and fluorescent imaging verification

To verify pattern transfer with the fluorescent PLL, the samples were imaged in LSM Zeiss confocal upright microscope with an excitation wavelength of 488nm.

For both micro-contact printed samples and insert samples, HL-1 cells were plated at a volume of $300 \, \text{cells/mm}^2$. Micro-contact printed samples were imaged after 4 days in culture (4 DIV) with Fluo-4 as described in section 3.2.2.1.

Insert-samples had the insert removed after 4 days in culture and were imaged with Fluo-4 after 5 days in culture.

3.6   Image-analysis

Two types of scripts were developed for the analysis of the acquired time lapse movies, one for single-cell signal analysis and one for wave propagation analysis. Development and analysis was performed in ImageJ (NIH, USA) run through Matlab 2012 (The MathWorks, Inc.) with a Miji–plugin that also enabled image processing prior to signal analysis.

3.6.1 Wave propagation analysis

The time lapse file was loaded into Miji, where a macro-script divided the movie into a matrix of regions of interest (ROIs), e.g. 25 x 25. A noise-reference-ROI (NR ROI) was selected with low cellular activity. The ROIs were run through the Miji Time series analyzer plugin to achieve a numerical signal vector for every ROI which then was loaded into Matlab.

The script developed to visualize the wave propagation was built upon the principle of cross-correlation using the Matlab-function *finddelay*. This function delivers the delay of a signal relative to a given reference and this is done by calculating the cross correlation between the signals and finding at which delay the cross correlation reaches its maximum value. If the signals are not relatable a 0 will be delivered. The temporal resolution for the delay is equal to the sampling time of the signal.

The analysis script was developed with the aim of displaying and plotting as much information as possible for the user once the signal files and parameters were loaded. The script flow is briefly described below.

The user loaded the signal files and gave, for example, temporal and spatial scaling parameters, time for stimulation, how many time-slots the signal should be divided into, ROIs for example-signals to display and a signal reference ROI (SR ROI) for the delay calculation.

When the script was run it calculated first the relative fluorescence intensity *I,* for every ROI according to Equation 1 where *s* is the signal vector, *n* is the NR ROI vector and *b* is the background as average of 30 first samples in the signal vector.

$$I = \frac{s-n}{b} \qquad\qquad \text{(Eq. 1)}$$

Thereafter, the signals were divided into a chosen number of timeslots in which all ROI signals were compared to the SR ROI by *finddelay*. The delays were then displayed in matrix-plots where the different delays were related to different colours. The use of several time-slots enabled the user to visualize the wave propagation at different times during the experiment. To achieve a readable propagation delay plot, the SR ROI had to be optimized for each individual experiment.

In the script, a number of ROIs could be selected for visualisation as example-signals. The signals were plotted in a separate window with markers for the duration of the stimulation. Markers for the chosen ROIs were also plotted in the propagation-delay plot to correlate the chosen example-signals with the propagation-delay plot.

A *findpeak* function detects and quantifies the number of peaks in the chosen example-signals. For each signal, the numbers of peaks before and after stimulation were extracted. To achieve average frequency values, the number of peaks was divided by the time duration before and after stimulation respectively. These frequencies represented the *activation frequencies* (AF) of the cells, which corresponds to a rate of action potential occurrence per second. The calculated AFs were displayed as a screen print-out. A students' t-test, performed with the *ttest2* function, on the 'before stimulation' and 'after stimulation' AFs gave a quick estimation if the AF had changed or not.

3.6.2 Single-cell signal analysis

The aim with this analysis was to investigate the response to electrical pacing on the cell at the point of stimulation (POS) and whether the stimulation activated the neighbouring cells.

Since the macro that creates the grid of ROIs caused binning of the signals, a second script was developed that displayed signals from single-cells only to achieve higher accuracy.

In this analysis process ROIs had to be placed manually over the cells of choice and could thereby ensure that the signal from only one cell was selected per ROI. The placement of the ROIs was done according to a zone-system to categorise the cell signal response in relation to its distance from POS. A circle with 20 μm in diameter was placed over the cell at POS. Around the POS-circle three more circles were placed with a radius of 30, 50 and 70 μm, respectively, thereby dividing the neighbouring cells into different zones. Zone 1 contained the cells closest to the electrode and zone 4 contained cells bordering or being in the close proximity to the outermost circle. If a cell was on top of the border it was considered to belong to the zone where majority of its cell body was. If it was equal in both zones it was categorised to belong to the inner one. An example of the zone-system is displayed in Figure 8.
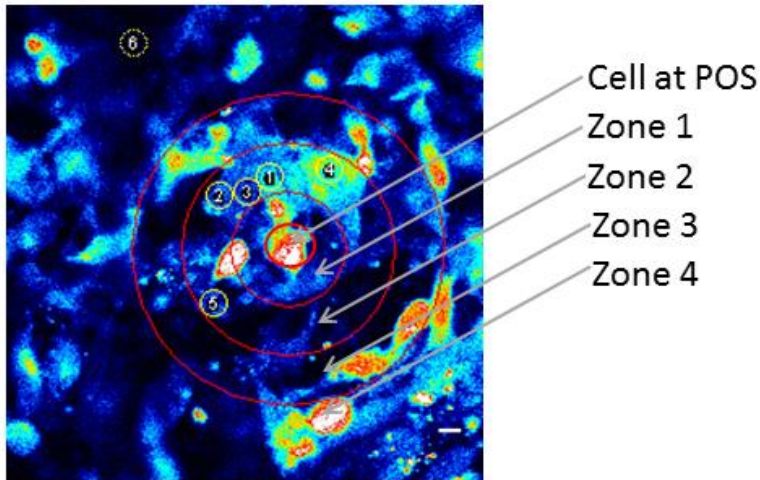
Figure 8. Single-cell analysis in zones. The signal analysis of the cells was done by comparing the response of the cell on top of the electrode with the response from the cells at different distances from POS. The inner circle marks the cell at the POS and the outer circles have radiuses of 30, 50 and 70 μm, respectively. The scale-bar is 10 μm. This image captures the ROIs, the small yellow circles with numbers, selected in zone 2. ROI number 6 is used as a noise reference in the fluorescence intensity calculation described in section 3.7.1.

To enable categorising of the signals and whether they were responding to the stimuli or not, three possible outcomes were defined.

The cell signal was considered:

- Elevated: if the base level of the signal increased more than 20% during stimulation.
- Distorted: if the standard deviation of the signal, which also accounts for its amplitude, changed more than 20% during stimulation.
- Paced: if AF increased more than 10% during stimulation.

If a cell signal exhibited any of these features it was considered as 'activated', combinations of these three outcomes were also possible.

The Matlab-script developed to extract the important parameters for this type of analysis was built on the same fluorescence intensity calculation as described in 3.7.1. The signal was divided into two segments where the first one contained the signal before stimulation and the second the signal during stimulation. The averages of the two signals were calculated with the *mean* function and the standard deviations with the *std* function. The AF before and during stimulation

was estimated with the *peakfinder* as described in 3.7.1. To find the relative changes in the parameters, the mean, the standard deviation and the AF value from during stimulation was divided with the corresponding value before stimulation.

All the AFs calculated in one trial from 'before stimulation' were averaged together with a standard deviation. The same was done for AFs after stimulation. These averages were referred to as *primary average frequencies.*

A number of cells showed irregular behaviour or had a noisy signal. These were excluded from the analysis according to following criteria:

- Low amplitude: if the cell had a standard deviation lower than 0.1 both before and during stimulation.
- Noisy or irregular: if the cell had an AF lower than 0.2 Hz both before and during stimulation.

Some cells showed a frequent beating signal but had irregular or regular peaks in the intracellular Ca^{2+} which occurred as peaks in the signal plots. An eventual distortion or elevation in these cells that was clearly not caused by the stimulation was not included in the result.

The cells were analysed following this protocol one zone at a time. The selection of trials was limited to experiments done with the low *f*-protocols in Table 1 with an image resolution of 10x, z1.2, z2 or 20x, z2. These resolutions gave a minimum scanning speed of 0.197 s for 10x, z1.2 and 20x, z2 and 0.156 s for 10x, z2.

The longest distance to an activated cell was also estimated. If an activation of a cell was seen in zone 4, the distance between the middle of the cell at POS to the middle of the furthermost activated cell was noted. If no activation was seen in zone 4 for a certain trial, the outermost zone with an activated cell was used. The longest distance for activation was then the distance from the centre of POS to the centre of the highest zone activated.

Finally a number of general AF parameters were calculated to determine a normal state for the culture. To achieve an estimation of the general intrinsic AF among the entire sample population that was analysed, all primary average frequencies were averaged into a *secondary average frequency* and its respective standard deviation was calculated. The highest and lowest primary average

frequencies, from before stimulation, were registered to complete the frame of the cell population activation behaviour.

3.7 Impedance measurements

Prior to the start-up of the pacing-project, a series of experiments were performed to examine the effect of stimulation on the impedance of the chip electrodes.

An already existing Matlab-script allowed the user to provide the numbers of the electrodes that were to be measured, and the script then called the software mentioned in section 3.3 to perform an impedance measurement on all the chosen electrodes. The measurement was performed at 7 values between 100-3000 Hz for each electrode and from these data a plot could be made.

However, to enable estimate the effect of stimulation on the impedance, the script needed further development. Therefore, a new Matlab-script was written which let the user chose one set of electrodes to be used for stimulation and one set to be used as control and load a number of stimulation-protocols associated with the electrodes that were to be stimulated. Moreover, the script let the user set the time of the experiment and how often the stimulation should occur. When the script was started it carried out stimulation on one electrode and directly after it measured the impedance. When the program had run through all the electrodes that were to be stimulated, it measured the impedance of the control electrodes.

The script was based on the Matlab *timer* and *callback* functions which enabled the timed execution of the stimulation and impedance measurement.

The stimulation protocols tested targeted different parameters of the stimulation such as different frequencies, voltages and repetitive long term stimulation. For long term stimulation experiments, the script was altered to test impedance only before the stimulation period started and after the period was completed. The protocols used are presented in Table 2.

Table 2. Stimulation protocols for impedance testing

Variable parameters	Fixed parameters	Timing	Impedance measurement
f: 5, 10, 20, 100 Hz	*A*: 250 mV *D*: 10 s PW: 0.2 ms	1 stimulation with every protocol, starting with the lowest *f*	After every frequency trial
V: 25, 50, 100, 200, 500 mV	*f*: 20 Hz *D*: 10 s PW: 0.2 ms	1 stimulation with every protocol, starting with the lowest *V*	After every voltage trial
	A: 500 mV *D*: 10 s *f*: 20 Hz PW: 0.2 ms	5 stimulations with the same protocol	After every trial
	A: 250 mV *D*: 10 s *f*: 20 Hz PW: 0.2 ms	4 stimulations per hour for 15 hours	Before and after long term stimulation
	A: 1650 mV *D*: 100 ms *f*: 500 Hz PW: 0.2 ms	1 stimulation	After every trial

The electrodes chosen for the impedance testing were selected from 4 different areas on the chip which all had the same nail height but different diameters. This variation was included to investigate whether the electrode dimensions affected recording and stimulation properties. In every area, 3 electrodes were chosen for stimulation and 3 as control samples. When displaying the results the data from the 3 stimulated electrodes was averaged and a standard deviation was calculated. The same procedure was followed for the control electrodes.

4 Results

## 4.1 The effect of plating density on the action potential and its propagation

The outcome of the plating density was based on the visual estimation described in section 3.4.1. The presence of regular intensity tops in the fluorescence associated with the action potential, appearance of the action potential waves, the viability and the occurrence of re-entrant spiral waves were as common in the high density as in the low density samples. The quality of the cells differed more in between cultures than between the different density samples. On the glass cover-slip samples it was observed that cell growth did not occur in only on but in two layers. When comparing coverslip samples with a high density-plating, 600 cells/mm^2, to samples with the standard plating-density, 300 cells/mm^2 it was noted that the total area covered by a double layer of myocytes was higher for the high-density plated samples. The double layer was not found on the chips.

4.2 The effect of patterning on action potential wave propagation

4.2.1 Micro-contact printing

The stamp-transfer control performed with FITC as described in 3.5.1.2 showed upon examination with fluorescence imaging that the pattern was transferred in all of the samples but to a different degree. The first and second sample, made from protocol 1, see section 3.5.1.2, showed a complete transfer of the grid-pattern with no broken lines, as shown in Figure 9 a). The sample from protocol 2 showed almost the same consistency in its pattern but as can be seen in Figure 9 b) there were patches that were slightly paler in intensity. The sample from protocol 3 had a clear grid pattern still visible but many of the grid lines were more or less broken, see Figure 9 d, e).

The trial with a cell culture seeded onto glass coverslips patterned with firbronectin showed tendencies to a structural arrangement at visual inspection in phase contrast microscope after 1 DIV. When the samples were imaged whith fluorescent imaging at 4 DIV the cells had reached full confluency and no indication of patterning could be seen.
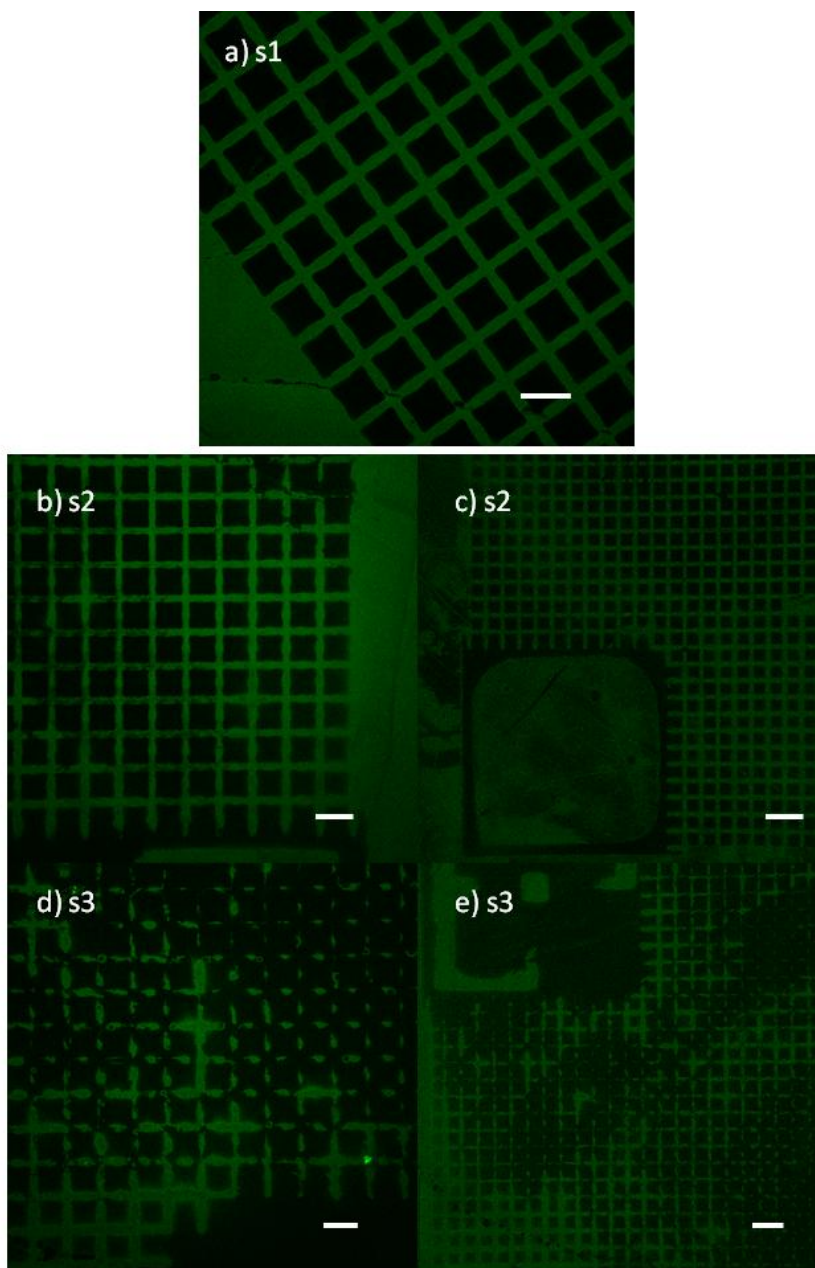
Figure 9. FITC-PLL images of micro-contact printed samples. The green grid shows how the FITC-PLL has been transferred by the stamp onto the cover slip. The scale bars are 100 μm in a, c, d) and 200 μm in d, e) **a)** Sample 1 shows an even transferred and consistent pattern. **b, c)** Sample 2 has a complete grid pattern but the grid lines are not even in their thickness. A darker streak can be seen in the lower left part in b) **d, e)** Sample 3 showed a very uneven pattern with many grid-lines broken or completely gone.

4.2.2 Patterning by silicone insert

Fluorescent imaging of the cells, loaded with Fluo-4, cultured on the chips with silicon inserts showed that most of the chip was free from cells except for some strands of cell clusters stretching from the side of the chip towards the middle in the direction of the insert-fingers. Nevertheless, the cells appeared to be viable in both samples, and showed frequent peaks in fluorescence and propagating action potential waves even in the strands on sample 2, Figure 10 b). Microscopy images of cells loaded with Fluo-4, and a photograph of the chip with an insert can be seen in Figure 10.
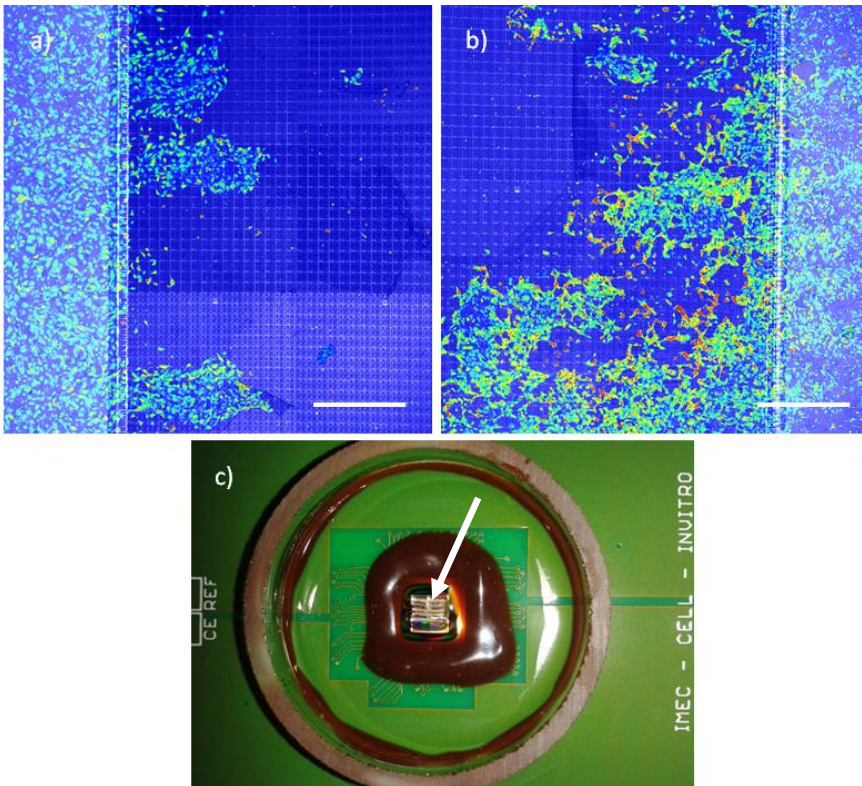
Figure 10. Silicone insert patterning. a) Sample 1. Combined snapshot with the chip-surface and a fluorescent caption of the patterned cells on top of the chip. The pale surface at the left is outside the chip and the checked pattern is the chip surface. Three strands of cells can be seen stretching in on the chip from the side. At this sample the cells looked healthy but did not yet show signs of propagating action potentials. **b)** Sample 2 is captured the same way as sample 1. At this sample propagating action potential were seen in the strand-like structures seen in the bottom left and in the middle of the image. For a) and b) The scale bar is 500 μm. **c)** A photograph of the chip with an insert-structure. The ring is the glass-ring that keeps the medium for the culture. The brown structure is epoxy painted around the chip to protect the wire-bonding. In the middle a pale branch-like structure can be seen which is the silicone insert. The arrow indicates placement of the insert.

4.3   Wave propagation analysis

Once the script for the action potential wave propagation analysis was finalised and put to use on the time-lapses recorded from the stimulation trials, a number of limiting conditions that determined the scripts functionality emerged.

- The spatial resolution was a crucial factor that determined if a propagating wave could be captured or not. The script developed could recreate the propagating waves into propagation-delay plots with time-lapses gathered with the 5x and 10x objectives while time-lapses captured with the 20x objective could not be used for making readable plots.

- The scanning speed versus the resolution was an important trade-off. If one zoomed in on the sample the scanning speed was increased which gave a higher temporal resolution for the signal but at the same time this meant a loss in spatial resolution if the wave was covering a large area.

- The quality of the culture was important, by means of confluency and successful loading of the Fluo-4, which determined the signal strength was important. A more confluent culture that was successfully loaded, thereby giving a strong and uniform signal gave better plots than those from more sparse cultures. These factors also determined in how many time-slots the signal could be divided, while still achieving a readable propagation delay plot. The higher the confluency and signal strength, the more accurate time-slots could be made.

- The appearance of action potential waves was crucial for the reconstruction of a propagation delay plot. If the waves were of such a size that a uniform wave front could be seen travelling across a sample area of 1213*1213 μm, which corresponded to time-lapse imaging performed with 10x objective, zoom 0.7 (z0.7), it was considered as big and uniform. This type of wave could be recreated into propagation delay plots even if it had some changes of direction. Action potential spiral waves could also be recreated at this sample size. On the other hand, if a sample of the same size had waves that came from multiple origins or had very fast directional changes, this could not be transferred into a propagation delay plot.

Based on the propagation-delay analysis from the initial stimulation experiments, an imaging area of 1213*1213 μm achieved with 10x objective, zoom 0.7 was considered the best trade-off for visualising the propagation of the action potential wave without binning too many cells together in each square in the matrix-plot. This was therefore the initial choice of resolution for time-lapse recording during stimulation experiments. An example of this type of plot can be seen in Figure 11.
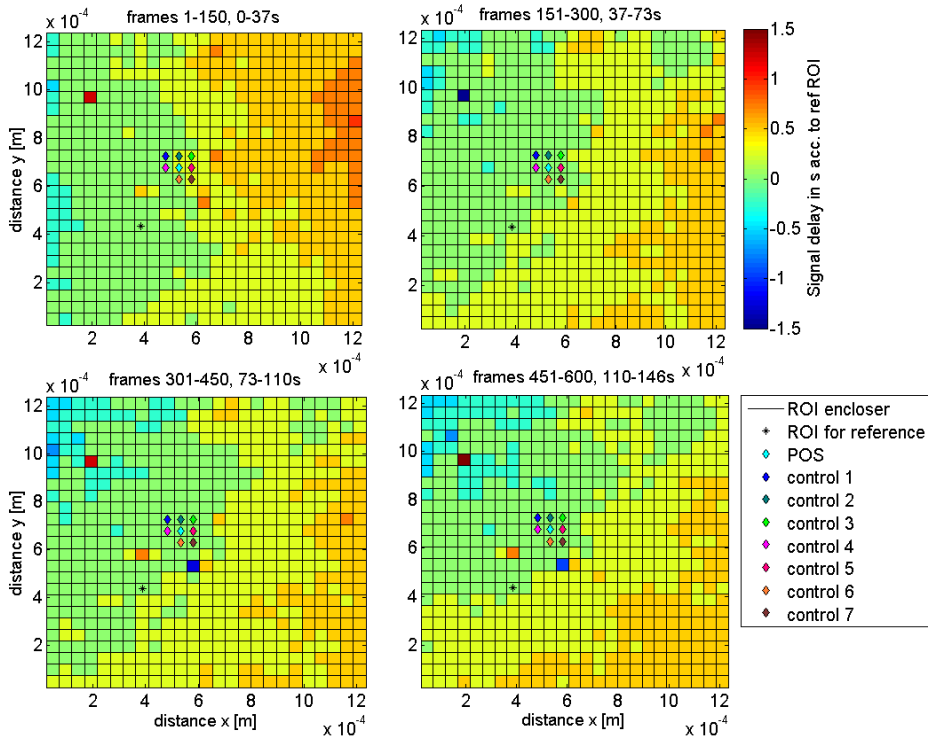
Figure 11. Example of a propagation-delay plot. The signal from the ROI with the black star was used as a reference to which all other ROI-signals were compared. The delays relative to the reference were colour coded according to the colour bar at the right. Blue hues indicate a negative delay, and yellow towards orange-red an increasing positive delay. The propagation of the wave can therefore be read as going from blue areas towards orange areas. The pale blue diamond marker shows the ROI containing the POS. Signals from the POS ROI and some of the neighbouring controls can be seen in Figure 12. This particular plot was made from a time-lapse recorded with the 10x objective, z0.7 which gave a frame rate of 4 frames/s. The stimulation protocol was 3 Hz, A:1.65 V, D: 30 s. In this example, stimulation started at frame 238, which corresponds to 58 s into the trial (plot 2) and ended 30 s later at 88 s (plot 3).

The plots in Figure 11 also exemplify a capture of a change of direction in wave origin. By comparing plot 1 to plot 2, 3 and 4 one can observe a shift of the blue area the left side to the upper left corner. Furthermore, an estimation of the

conduction velocity can be done from the plots in Figure 11. The frame-rate of 4 frames/s translates in each 'delay-step' to be 0.25 s. This indicates that a wave going from blue to dark orange, as in slot 1, will pass 4 delay-steps, which sums up to 1 s in propagation time going from left to right. Taking this time and dividing it by distance travelled, an average speed of 1213 µm/s can be calculated

During the analysis of the propagation delay from the stimulation experiments it became clear that the local stimulation did not affect the propagating action potential waves to such an extent that it could be distinguished as a change in the propagation delay plots. Although, in many trials, the signal plots from the sites at and around the POS showed that these cells were responding to the stimulation with an elevation in base-level or a distortion of the signal. An example of signal plots achieved with the propagation-delay script can be seen in Figure 12.
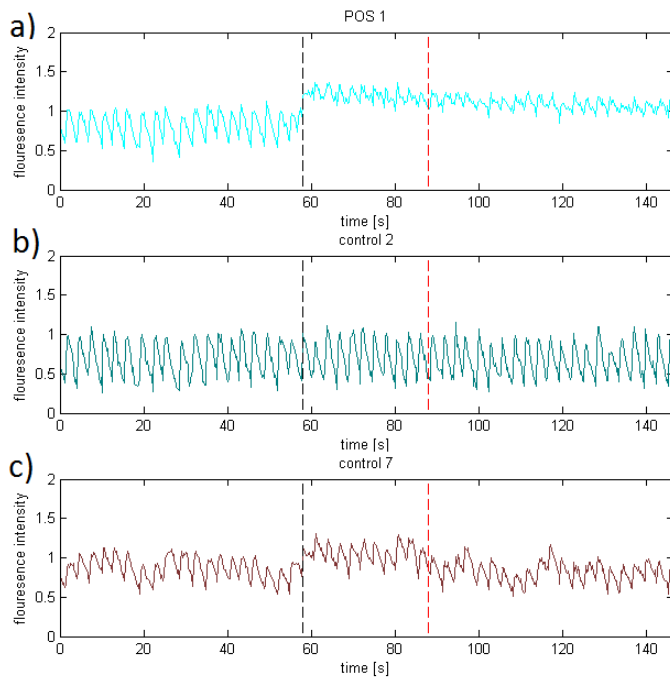
**Figure 12. Selection of signals from the propagation-delay plot.** A selection of the signal displayed with the propagation-delay script that corresponds to the ROIs for the POS, control 2 and control 7 in Figure 11. The black and red dashed lines show the start and end of stimulation. From the plots it is clear that an elevation of the base level of the signal occurs at POS and in control ROI 7 but not in control ROI 2.

4.4 Single-cell signal analysis of pacing protocols

The data from the single-cell signal analysis is summarized in the following graphs. The data was normalised to the total number of cells per zone or pacing frequency depending on plot type and presented as percentage values.

The different types of activation, elevation, distortion, AF increase and their combinations are stacked into bars to display their distribution in relation to the total number of activated cells.

To visualise the spatial spread of the activation among the cells due to electrical stimulation, the responses from all pacing frequency protocols, 1 - 5 Hz were binned together and displayed per zones, as shown in Figure 13. In this plot, 100% corresponds to the total number of cells in the zone that were analysed. From the plot in Figure 13, it could be observed that the percentage of activated cells decreased almost linearly with the distance from the POS, with only a slight deviation for Z2. The maximum activation was seen at the POS, which reached 80 % activation, while the outermost Z4 only reached 20 %. Two trends within the distribution of the different activation types could also be distinguished. Firstly, activation responses that included elevation of the base level were mostly localized to the POS and the innermost zones. Secondly, responses with multiple activation criteria fulfilled, such as 'elevation and distortion' tended to be more common for the innermost zones
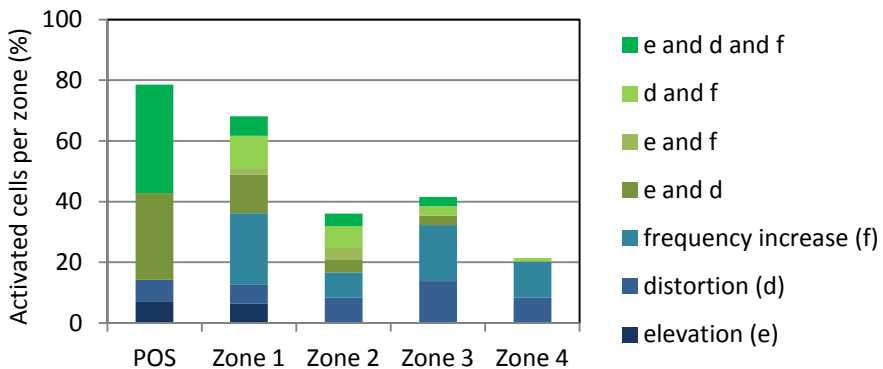
Figure 13. Activated cells per zone. Each zone includes the cells from all the pacing protocols, 1 - 5 Hz. Total number of cells analysed per zone are: POS = 14, Z1 = 47, Z2 = 72, Z3 = 65, Z4 = 84 and corresponds to the 100% value. A decreasing trend in percentage of activation can be seen going from the point of stimulation (POS), which had almost 80 % cells activated, and outwards to zone 4 which had just above 20 % cells that were activated by stimulation.

The distribution of the activation responses for different frequency protocols were displayed for the cells at the POS and for the different zones respectively as shown in Figure 14 and 15. In these plots, 100 % for every bar corresponded to the number of cells analysed for one specific frequency protocol in one specific zone.

The plot in Figure 14 shows that not all cells at POS were activated since the neither of the bars at 1, 2 or 3 Hz reached 100% activation. As mentioned above, activation by multiple fulfilled activation criteria seemed to be the dominating response type.
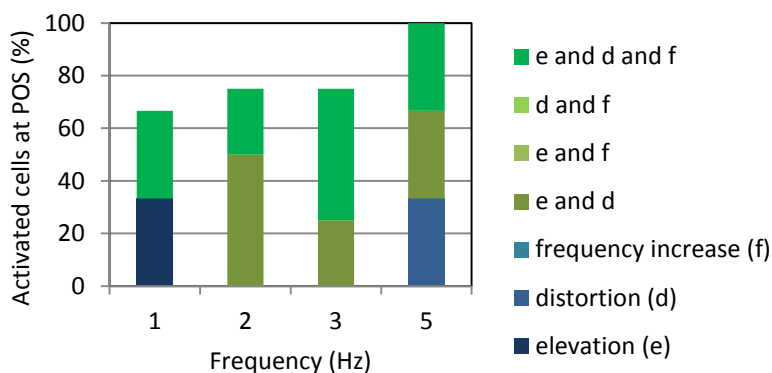
Figure 14. Activated cells at the POS per frequency protocol. 100% corresponds to the total number of cells at the POS for a specific pacing frequency. The total number of cells analysed per protocol was: 1 Hz = 3, 2 Hz = 4, 3 Hz = 4, 5 Hz = 3. As can be seen there were cells at POS that were not activated since all bars did not reach 100 % activation.

In Figure 15, all 4 zones and their respective activation responses distributed over the different frequency protocols are shown. The separation of the frequency protocols showed no clear trend in deviation in percentage of activation related to the pacing frequency of the applied stimuli.

In Z1, Figure 15 a), the percentage of activation was around 60 % for 1, 2 and 5 Hz but all up to 80 % for the 3 Hz protocol. In Z2, Figure 15 b), the percentage of activation showed a slight increase with increasing stimulation frequency where 1Hz showed 30 % activation and the 5 Hz protocol caused almost 50 % activation. Z3, Figure 15 c), showed the largest deviation in percentage of activation between the different protocols. The 3 Hz stimulation caused almost 60 % activation while the 2 and 5 Hz protocols only induced 25 % activation and the 1 Hz protocol ended up in around 50 % activation. Finally, Z4, Figure 15 d),

showed the smallest deviation in activation response which was around 20 % for all the protocols. A clear trend in response related to the stimulation frequency could not be observed within these graphs.
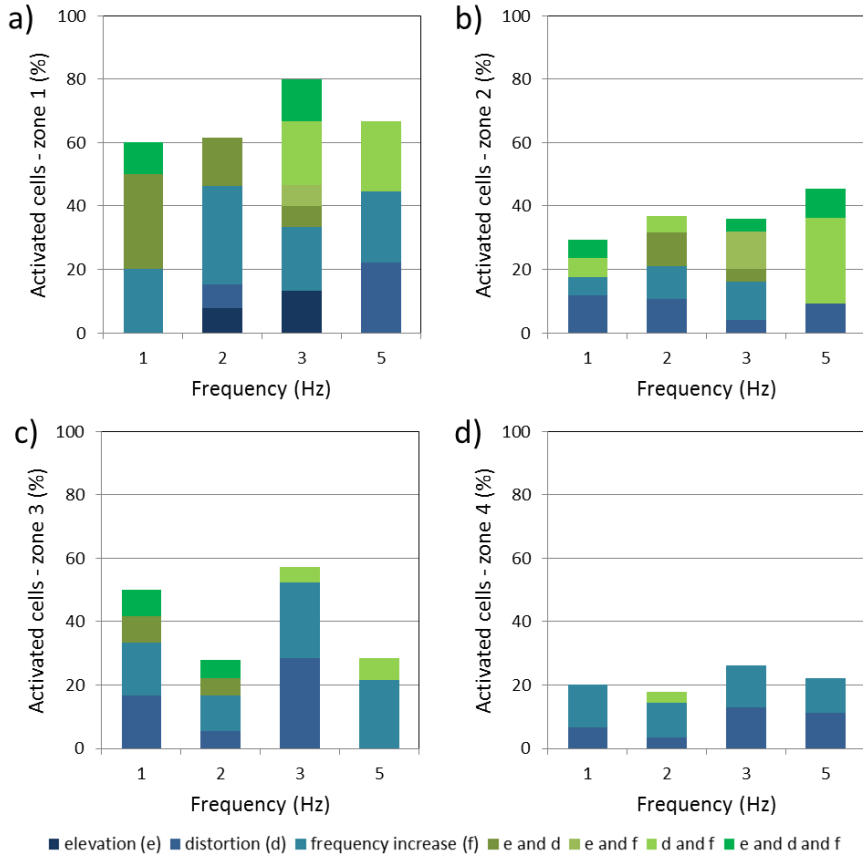
Figure 15. Activated cells in zone 1-4 per frequency protocol. 100% corresponds to the total number of cells in the zones analysed for a specific frequency protocol. Total number of cells analysed per protocol are given per zone and pacing frequency **a) Z1:** 1 Hz = 10, 2 Hz = 13, 3 Hz = 15, 5 Hz = 9. Overall activation per frequency protocol is 60 % or more for all protocols. **b) Z2:** 1 Hz = 17, 2 Hz = 19, 3 Hz = 25, 5 Hz = 11. Overall activation is between 30 − 45 % for all frequency protocols. **c) Z3:** 1 Hz = 12, 2 Hz = 18, 3 Hz = 21, 5 Hz = 14. With an overall activation varying between 25% for the 2 Hz protocol to 55 % for the 3 Hz protocol the difference between frequency protocols is higher than for the inner zones. **d) Z4:** 1 Hz = 15, 2 Hz = 28, 3 Hz = 23, 5 Hz = 14. Overall activation is just under or just above 20 % for all frequency protocols.

To exemplify the spreading of the activation from POS to the different zones, the signals from one trial that exhibited activation in cells in all the zones was showed in Figure 16 a). To facilitate the read-out of the time of activation, the signals were filtered in Matlab prior to plotting. From the plot, the maxima in elevation was extracted and occurred at: 40 s, 42 s, 43 s, 47 s and 55 s for the cell at the POS and the cells in zone 1-4, respectively. The orientation of the cells relative to the POS is shown in a caption from the time-lapse in Figure 16 b).
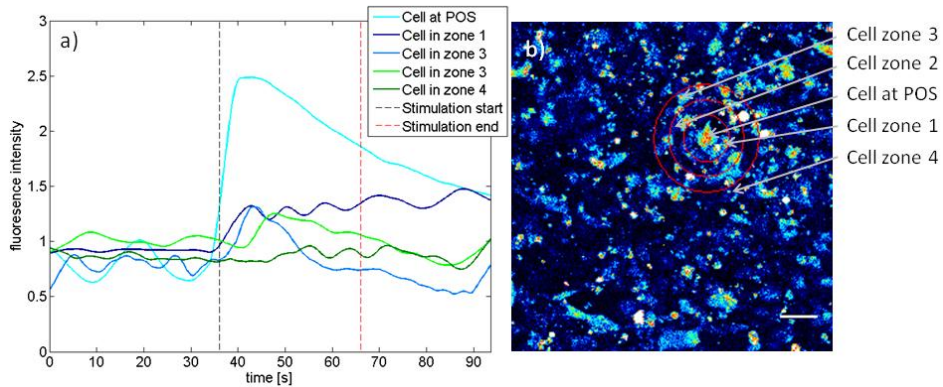
Figure 16. Example of delay in activation for different zones. A) Plot of signals from the cell at the POS and activated cells from every zone. The signal was filtered in Matlab to visualise the activation by elevation or distortion in signal. The maxima in elevation occurred at 40 s, 42 s, 43 s, 47 s and 55 s for the cell at POS, zone 1, 2, 3 and 4 respectively. **B)** The position of the cells which signals are plotted in a) are displayed with a caption from the time-lapse. The scale bar is 50 μm.

The calculated average of the longest distance between the POS and an activated cell distributed over the different frequency protocols is shown in Figure 17 together with respectively calculated standard deviations. A total average including all frequency protocols was also provided with the graph. From the plot in Figure 17 it was observed that the protocols for 1, 3 and 5 Hz all showed a longest distance to an activated cell just around 70 μm which was also the average for the total average calculated. The result for the 2 Hz protocol deviated from the others and had a longest average distance of almost 80 μm to the furthest activated cell. This sample population (2 Hz) did also show the largest standard deviation. The number of cells measured per protocol were: 1Hz = 3, 2 Hz = 4, 3 Hz = 4, 5 Hz = 3, which made a total of 14 cells.
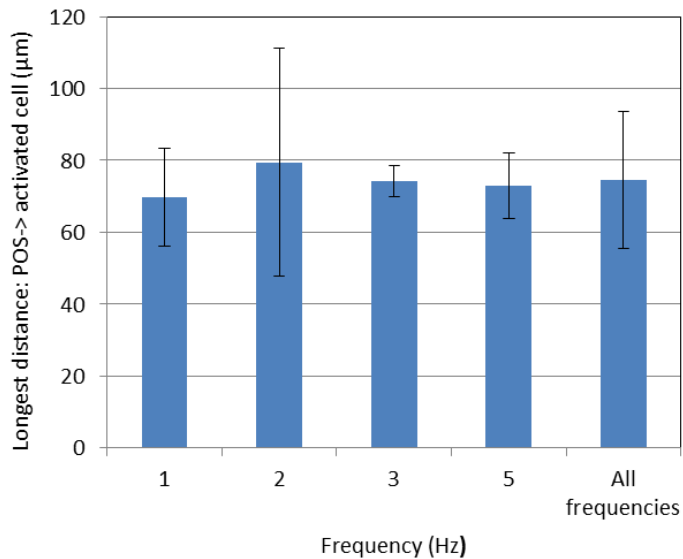
Figure 17. Average distance from POS to the outermost activated cell. Average distance and the standard deviation calculated to the outermost activated cell relative to the POS centre for every frequency protocol. A total average including all frequency protocols is labelled 'All frequencies'. The number of cells per frequency protocol was: 1Hz = 3, 2 Hz = 4, 3 Hz = 4, 5 Hz = 3 and total number of cells was 14.

The cells that experienced any AF increase higher than 10 % during stimulation were classified as paced. For each frequency protocol, the relative AF increase was averaged and displayed with the respective standard deviation, which is showed in Figure 18. The sample population included all cells classed as paced in all zones, excluding POS. The average AF increase was around 20 % for cells activated by the 2, 3 or 5 Hz protocols but the respective standard deviations were almost at the same value. The large deviation for the 1 Hz protocol, which showed an average increase of 45 %, was mainly caused by one sample that deviated from the others. The sample cannot truly be classified as an outlier since the large increase was a result of a low AF before stimulation. If however, this sample was to be removed the average AF increase for the 1Hz protocol would be 30 ± 19 %.
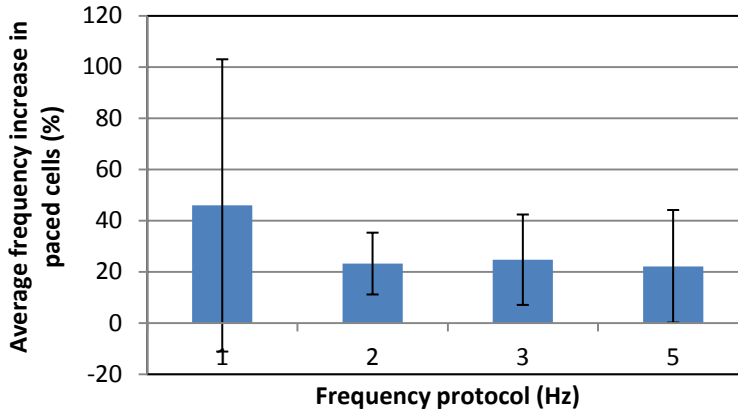
Figure 18. Average activation frequency (AF) increase for paced cells. The graph displays the average increase in percent with the respective standard deviation for the cells classified as paced. The sample include cells activated by displaying an AF increase in all zones, excluding the POS. The number of cells per protocol was: 1 Hz = 11, 2 Hz = 15, 3Hz = 24, 5 Hz = 14. For the 2, 3 and 5 Hz protocols the average AF increase was just around 20%, a value from which the 1 Hz protocol deviated and showed an average of 45 % increase.

The intrinsic rate of AF among the entire sample population before stimulation is shown as the secondary average frequency in Table 3. This secondary value was derived from an average of all the primary averages from before stimulation, as stated in section 3.6.2. To compare the range the primary average frequencies occurred before stimulation, the highest and lowest observed value are also shown in Table 3.

Table 3. General activation frequency parameters of the cells calculated on the frequencies obtained before stimulation.

	Activation frequency (Hz)
Secondary average frequency	0.73 ± 0.15
Highest observed primary average frequency	1.14
Lowest observed primary average frequency	0.43

A dose-response curve could not be achieved due to a too low sample number. However, the very lowest voltage applied that caused activation in the cell at POS was 1 V and was achieved with a 5 Hz protocol.

4.5 Single-cell signal analysis of blocking protocols

The number of high resolution samples was very low (n=5) and initial screening of the signal response showed large deviations between trials. For this reason the script which was previously used for more detailed analysis of the pacing-protocols, was not applied to the high-frequency protocols. However, the initial signal analysis did show that elevation and distortion of the signal for the cell at the POS is possible to achieve with high frequency stimulation. The same features were also observed in a number of cells neighbouring the POS. Moreover, multiple activations due to repeated stimulation could also be observed. The described signal responses can be seen in Figure 19.
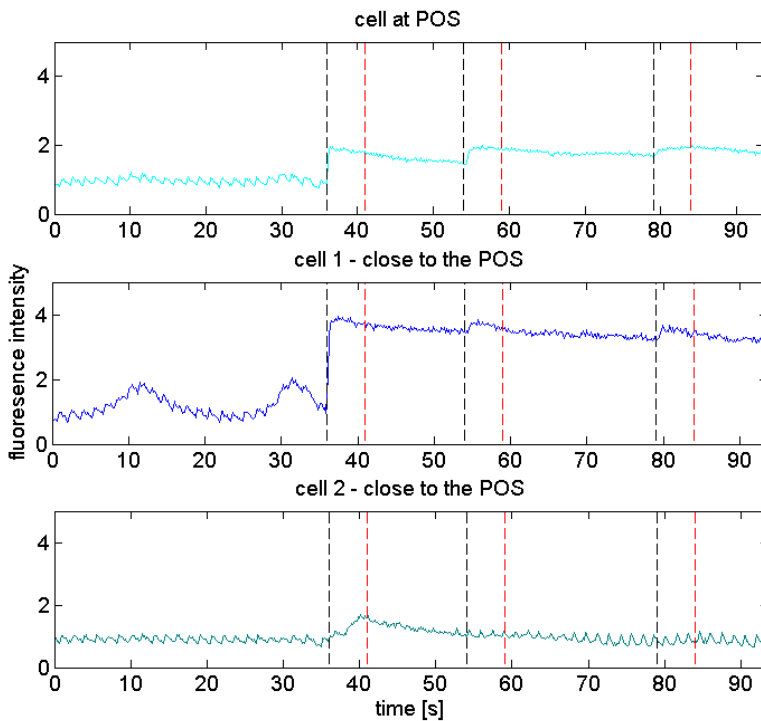
Figure 19. Example of blocking protocol single-cell response. In the caption, single cell response from a cell at the POS and two of its neighbours is showed. The blocking protocol used was *f:* 1 kHz, *A:* 1.65 V, *D:* 5 s and it was applied three times during the time-lapse recording. The black vertical lines marks stimulation start and the red lines the stimulation end. For all three cells, regular occurring peaks in the signal can be observed before the first stimulation. At the first stimulation, all three cells showed an elevation in base-level and a distortion in the regularity of the occurring peaks. The cell at the POS and cell 1, the first neighbour, showed a maintained distortion plus elevation on the second and third stimulation. Cell 2 only showed an elevation and distortion on the first stimulation occasion. These are visual observations on one sample to show as an example on signal response and have not been quantified with the same method as the signals from the pacing experiments.

4.6 Propagation delay analysis for sequential stimulation protocols

The execution of the sequential stimulation proved to be difficult in terms of consistency since the manual clicking to switch electrodes could not be timed efficiently. Hence, only a small number of trials were performed for this experiment.

Since the aim of the sequential stimulation was to investigate whether it caused a change in action potential wave propagation, these experiments were captured with low-resolution time-lapses, (10x objective, z0.7) which made single cell analysis impossible. Since the duration of the pulse-train also was short, 0.5-1 s, a detection of the signal in the example-signal plots achieved with the propagation delay-script was challenging. This left only the propagation delay-plots to be used for analysis of activation.

In the majority of the samples captured, no obvious changes could be detected in the action potential waves when transferred to propagation delay-plots. Although, one sample did show a change in its pattern occurring at the same time as the on-going stimulation, see Figure 20. The change displayed as an altering of the colour at some of the ROIs were stimulation occurred. The colour was altered so that it indicated that the signal in that ROI had a higher delay during the simulation than before.
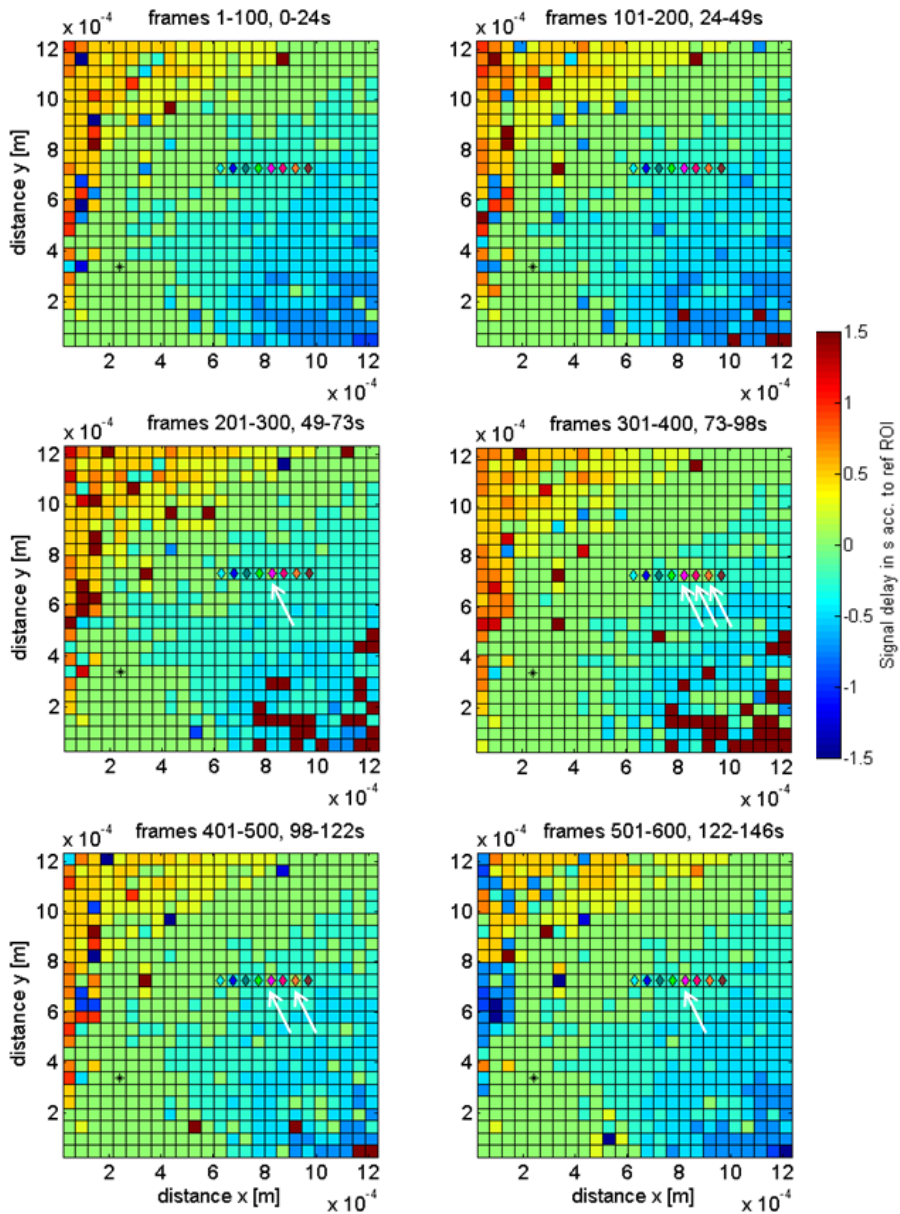
Figure 20. Example of propagation delay during sequential stimulation. Stimulation occurs in the ROIs marked with diamond markers in sequence moving from the left-most marker to the right. The first sequence-stimulation started at frame 217, which occurs at slot 3. Second sequence started at frame 420, slot 5. Note that some of the ROIs with markers are green in slot 3, 4, 5, (marked by arrows) and which are right after the first and during the second stimulation sequence but blue in slot 1 and 2. This indicates that the signals under the ROIs would have a higher delay in slot 4, 5 and 6 compared to the earlier slots 1 and 2. The ROI marked with a black star was used as a reference ROI for the delay calculations.

58

4.7 Effect of stimulation on electrode impedance

The results of the impedance measurements performed to investigate the effect of different stimulation protocols on the Neuray-II chip electrodes were all very similar. All graphs showed an appearance similar to the one put as an example in Figure 21. The interpolated lines were all on top of each other and the error bars were overlapping. No relevant difference was observed between electrodes that were stimulated and electrodes that were not stimulated. This was valid for all the different protocols and parameters tested.
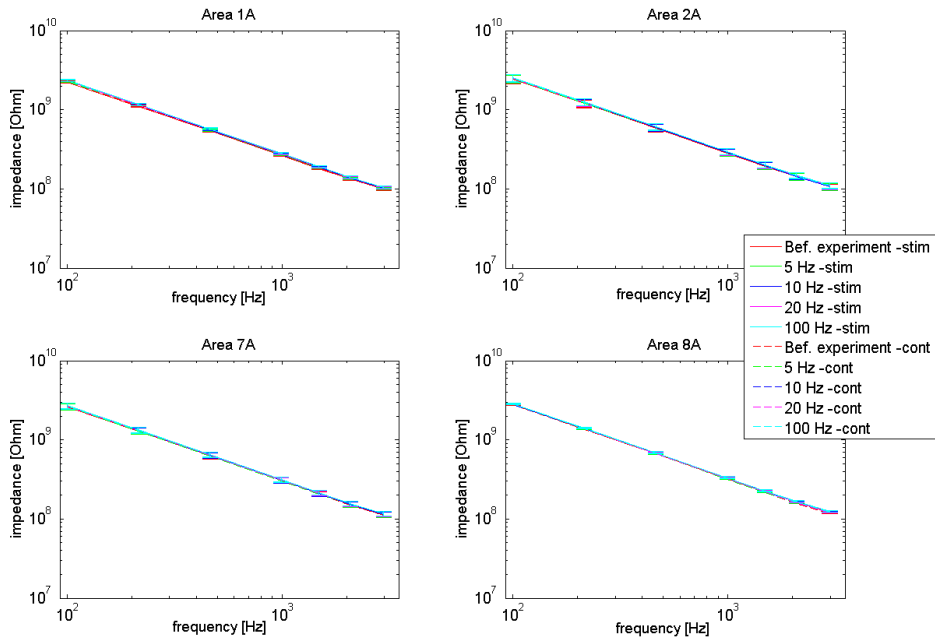
Figure 21. Example of impedance measurement graph. Evaluation of varying frequency protocols. The general appearance for all of the different protocols examined. No relevant difference can be seen between stimulated and non-stimulated electrodes.

The only graph that showed any degree of change at all was the one for the over-night stimulation protocol. The displayed change was not however between stimulated and non-stimulated electrodes but rather between before and after the stimulation experiment. As can be seen in Figure 22 for the high frequencies at area 8A, there is a difference between the impedance value before stimulation start and after experiment was finished. This is true for both stimulated and non-stimulated electrodes.
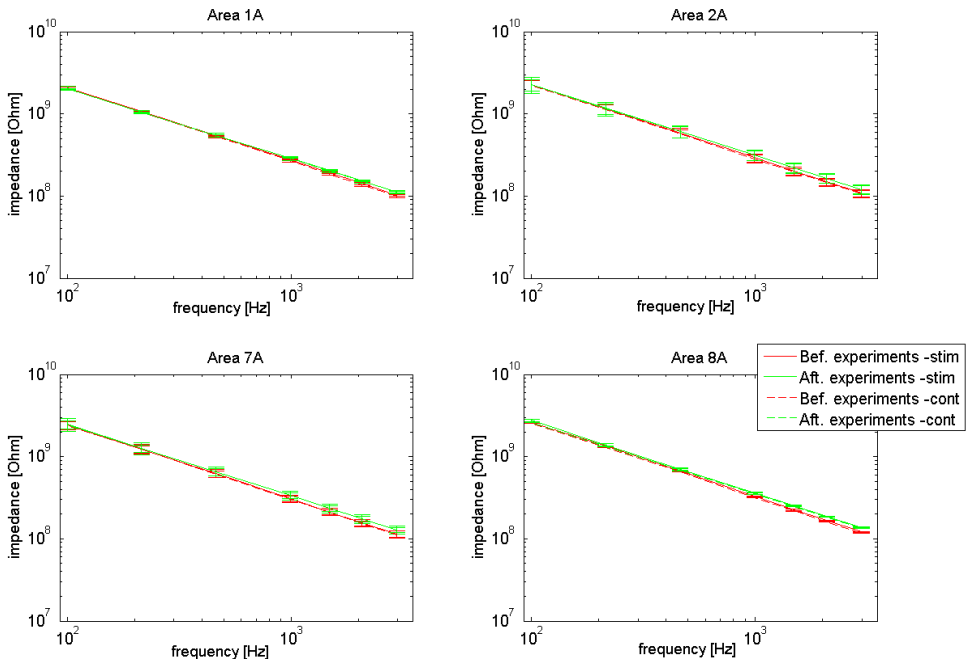
Figure 22. Impedance measurement before and after long-term stimulation. A small difference can be seen when comparing impedance before and after stimulation, especially for the higher areas 7A and 8A, which have larger diameter in their electrodes. The difference is most obvious for the higher frequencies.

5 Evaluation and discussion of the results

The discussion-chapter is divided in two main subsections. The evaluation of experiments and analysis methods related to large-scale effect on the propagation of action potential are gathered under "Macroscopic effects on the action potential and its propagation". The results from the analysis performed on a cellular level are discussed in "Local effects on the action potential propagation". Lastly, the results from the impedance-experiments will be evaluated.

5.1 Macroscopic effects on the action potential and its propagation

5.1.1 The effect of plating density

The reason that different plating densities of cells were investigated was that Hong and co-workers claimed that a plating density lower than 500 cells/mm^2 would not result in any stable spontaneously occurring re-entry spirals for HL-1 cells [21]. Further on they also claimed that cell viability was at its peak after 48 h in culture which corresponds to only 2 DIV and that this also was the earliest where spiral re-entries could be detected. In the conclusion from Hong and co-workers they state that the HL-1 cells should not be used for more than 3 days for studies of re-entries. Since these recommendations deviated from the normal in-house procedure for HL-1 i.e. a plating density of 300 cells/mm^2 and experiment after 4-5 DIV, a comparison of high and low plating densities and its effect on the occurrence of re-entrant spirals was performed. As mentioned in the results section 4.1 no clear difference was observed between the two densities tested. Spirals were observed as early as 4 DIV in samples from both plating densities. Since Hong and co-workers observed re-entrant spirals as early as after 2 DIV [21] it would have been of interest to investigate whether this was the case in our study as well. The reason for why no experiments were performed at this stage was that this study was limited to the use of calcium imaging for caption of the action potential waves. Earlier in-house experiments had not provided acceptable captions of the action potential waves until at the 4 DIV which is why no experiments during earlier stages were prioritised within this study. Hong and co-workers, on the other hand, had access to the propagation-induced phase contrast imaging system [22] described in section 2.3.3.2, and achieved their result by observing contractile motion and not intracellular calcium changes as in our case. Whether the re-entrant spirals could be observed with calcium imaging at 2 DIV or if it is only possible with the propagation-induced phase contrast imaging system is still to be seen.

Due to the lack of the instrumentation that can be used for non invasive long-term observation to determine the development of the cellular population, further investigation of this topic was not prioritised for the study. However it is notable that a double layer of cells was not observed to the same extent on the chips as on glass cover-slips which might indicate that the patterned chip surface affected the development of the cell culture. To verify the developmental stages of the culture both on chips and cover-slips and the detailed affect on action potential propagation and spiral induction, long term observation needs to be carried out in a non-invasive way, for instance as Hong and co-workers did, described in 2.3.3.2. One would preferably complete this with live-dead stainings and cell counts to determine the viability of the cell culture for different plating densities and on different surfaces (chip or cover-slip) to further rule out what plating density and number of days in culture is required to achieve spontaneously occurring re-entrant spiral waves. This can be of importance for *in vitro* modelling both if the goal is that re-entrant spirals occur spontaneously as well as when one does not want them to occur.

5.1.2 The effect of pattering

Neither the patterning with micro-contact printing or with the silicone insert showed any successful results in affecting the propagation of the action potential wave propagation. One of the primary reasons for why none of the methods could produce a pattern that caused a structural pattern in the culture, without completely removing the properties of a cellular network, was that the scale of the pattern was not on the scale of the cellular network.

In the case of micro-contact printing, it can be seen in Figure 9 in section 4.2.1 that the grid pattern encloses square of around 100 μm, which makes the grid lines to be approximately 20 μm in width. As can be seen in Figure 8 in section 3.6.2, the cell core if an HL-1 cell is around 20 μm in diameter and the cell body itself normally stretches even a bit further than that. This means that the cells could only have fitted into the grid-line if they would have attached as a single row, one cell after the other. This might have been the case in a very early stage of the culture since a slight structural growth could be observed during the visual inspection after 1 DIV. However no experiments with Fluo-4 Ca^{2+} imaging were performed at this stage that could confirm this since the Ca^{2+} peaks that indicated action potential firing normally not is seen this early. When imaging the samples at 4 DIV, traces of the patterning could not be seen either in the cellular network structure or in the pathway of the propagating action potential waves. The reason for this is most probably due to the cellular growth

mechanisms. At the early stages of the culture the fibronectin-coated areas plays an important role for the adhesion of the cells since it offer an increased cell-substrate adhesion by introducing ligands that the cell can attach to [64]. However, when the cells keep on dividing they are forced to seek growth space outside the coated grid-lines. It seems though as the importance of a coated surface is highest just after plating. As long as some cells could attach initially they seem to give each other enough support to maintain cell growth and keep spreading at later stages even if the surface does not provide ligands that facilitates attachment. No verifying experiments were performed, but for all samples, the whole cover-slip was covered with cells at the day they were imaged. Since no coating was applied in addition to the one applied with the stamp, this gives an indication that the coating is not necessarily of high importance to the growth of the cells. The outcome of the experiment might have been different if a larger pattern was applied, as the one used by Bian and co-workers [24], see Figure 4 d). Bian's sample preparation also differed to ours in terms of pre-coating of the sample with PDMS, printing time up to 40 min and blocking of non printed areas with 0.2% (wt/vol) Pluronic F127 for 20 min. These are printing parameters that could be explored further. It is although questionable if PDMS coating would be used for patterning on the chip surface since it would worsen the cell-electrode interface. With the use of HL-1 it would also be of interest to investigate if addition of components that inhibits cell division, such as Arabinofranosyl Cytidine (AraC), would improve the cell-network's adaptation to the printed pattern.

However, regarding this study, no other suitable wafer to be used as a stamp master was available, which is why these experiments were not continued.

With the case of silicone inserts, the effect was rather the opposite. The size of the grid constructed was too large to let the cells form a network. As can be seen in Figure 10 in section 4.2.2, only a few strands managed to form in between the legs of the grid-like insert and the spacing between these strands were too large to allow any interaction strand-to-strand. One reason that the strands did not grow further could be that the insert was dipped into PDMS before placing onto the chip and this PDMS might have floated out to cover the chip-surface between the insert legs and thereby prevented any cell attachment and growth. The limited amount of time prevented any refinement of this patterning method but as a future development it would be possible to create a finer insert which could allow a better cell growth around the structure. Another method for attaching the insert to the chip would also be preferred since the PDMS most

probably was a major contributor to the low cellular attachment. A more viscous substance would be a better choice. Some type of grease could be used since it is still sticky and does not float out like the PDMS. Usage of grease as attachment would not require curing in the oven either, which PDMS does, thereby sparing one extra step in the experimental process. Vaseline could be a possible option to be used for this purpose. Vaseline is considered non-toxic and have been used both in coating-preparations and as sealing substance in patch clamp experiments [65, 66].

5.1.3   Usability of the wave propagation analysis script

As stated in section 4.3 there were no macroscopic changes detected due to electrical stimulation in the propagating action potential waves within the propagation delay plots acquired. However, the lack of results might be dependent on the nature of the localised stimulation rather than the analysis method, which will be discussed further in section 5.2.

Even if no change in action potential wave propagation related to stimulation was detected, the analysis script still fulfilled its purpose of displaying the action potential wave during different time-slots of the experiment. The main requirement is that the culture is confluent and viable enough to give a stable and strong signal from the Fluo-4 loading. This is a requirement of the culture that is desired in any case since it provides a good base level in cell quality for performing experiments.

If this requirement is met and the spatiotemporal resolution of the captured time-lapse is set so that a propagating wave can be captured, this propagation can be re-created with the propagation delay-plots in an accurate way. As already stated in section 4.3 it was possible to re-create both directional changes in wave propagation as well as re-entrant spirals and the better the culture and signal quality were, the more time slots the signal could be divided into allowing a more detailed temporal analysis.

In our case, it was the imaging rather than the script that limited a higher resolution wave propagation analysis since the calculation of the delay was dependent on the frame rate. When imaging an area of 1213*1213 μm^2 or larger the frame-rate of 4 frames/s was usually enough to re-create the action potential wave. These settings provided plots that displayed the propagation of the wave in up to 5 delay-steps when the velocity of the wave was around 1213 μm/s, see Figure 11. If an action potential wave with the same velocity, should be described in a propagation delay plot but on a higher magnification the frame-

rate would need to increase linearly with the decrease of image size to be able to maintain the spatiotemporal resolution. As an example, if a wave with velocity of 1213 μm/s should be re-created into a propagation delay plot from a sample area of 606.5*606.5 μm^2, a frame-rate of at least 8 frames/s would be needed to maintain the 5 delay-step accuracy. For our microscope, the frame-rate did not increase linearly with the zoom and a top speed of 0.156 s per frame set our maximum frame-rate to 6.4 frames/s, thereby also limiting the usage of the propagation delay script to the low resolution captions.

Even if the script is overall functional, at least two refinements could be done to improve readability and accuracy and they are both related to the performance of the *finddelay* function.

- If the *finddelay* function finds that the two signals it is comparing are not correlated it will deliver a zero as delay. This zero-value cannot be separated from the zeroes delivered from an actual zero-delay calculation which introduces an inaccuracy to the script in its current form. Preferably, this would be altered so that a 'Not-a-number' (NaN) or a high or low extreme value would be returned by the function in the case of no-correlation occurrence so this could be displayed with a separate colour and thereby re-creating a more specific caption of the wave propagation. An implementation of this accuracy check would require quite some additional work with the code. Since the initial results from the propagation-delay plots did not show any clear changes to our samples during applied stimulation, an implementation of this function was not prioritized within the time limits of the project.
- The second inaccuracy is due to the *finddelay* handling of periodic signals. As mentioned in 3.6.1 the *finddelay* will return the delay value for which the highest cross-correlation is achieved. However, when comparing periodic signals, including our signal which had regularly occurring peaks, many delay-values will give the same absolute value for cross-correlation. The *finddelay* function handles this by returning the lowest delay achieved as a negative value. This introduces an inaccuracy so that areas that should have had a high delay value and been displayed as dark red, are instead displayed with blue hues that are given by their negative sign. Usually this inaccuracy can be recognized as faulty in the propagation delay pattern by observing the rest of the plot. A normal wave usually has the directionality of going from pale blue to green, yellow, orange and then red. If the same order of colour is

appearing in the plot displaying a wave-propagation but ending in dark blue instead of red, a periodicity inaccuracy has occurred. As said this inaccuracy is usually easily spotted by the observer but to have a decent analysis tool this should be corrected as well. Although, the solution for this issue is more complicated than for the previous one. Here, one would need to implement some sort of function that compares the delay calculated for the ROI of interest with the delays calculated for the neighbouring ROIs. Depending on the outcome of the neighbouring ROI-signals it could be determined if the delay should be displayed as highly negative or highly positive.

When putting this analysis method in the context of other high-end imaging resolutions as the contact fluorescence imaging system developed by Tung and co-workers [45] and the phase contrast imaging developed by Hwang and co-workers [22], described in 2.3.3.1 and 2.3.3.2 respectively, it does not strike as a very competitive alternative. Tung's system offers a far higher temporal accuracy with a sampling rate in its array system of up to 1 kHz. Hwang's system has a similar temporal resolution as our system with its time-difference imaging being performed on the 100 ms scale, however the system has the highly important feature of being non-invasive since no dye is needed, thereby allowing long-term experiments.

Although, our analysis system provides two other important features. Firstly, it offers a higher spatial resolution. Both Tung's and Hwang's system operates on samples that are around $10*10$ mm^2 in area but by using a confocal microscope and the script developed we can observe wave propagation and spiral structure on samples as small as $1213*1213$ μm^2 ($\approx 1.21*1.21$ mm^2). If imaging sample rate could be improved it is most likely that even smaller samples could be re-created as propagation delay plots accurately. Secondly, this method is relatively user friendly by not requiring the highly specialised instruments as the ones developed by Tung and Hwang. We have achieved the basics to a decent analysis system by using conventional Ca^{2+} imaging with a confocal microscope and a self-developed Matlab-script. These are instruments and techniques that are commonly used among labs and would therefore not require a lot of extra resources or time to implement.

5.1.4   The effect of sequential stimulation

The few trials with the sequential stimulation were our last attempts to see if a macroscopic change could be achieved in the propagation of the action potential. The idea was to try to create a block for the propagating action potential wave by

quickly stimulating a row of electrodes by using a high frequency protocol and thereby to resemble the blocking experiment performed by Dura and co-workers [25]. As mentioned in section 4.6, the method turned out to be difficult to manoeuvre in a systematic way and since the propagation-delay analysis plot did not show any clear effect, a refinement of the stimulating technique was not prioritised for further development due to the limited time of the project.

Although, there are some indications that points toward a possibility to block the action potential by using high frequency stimulation protocols, which will be discussed further in section 5.2.3.

If further experiments would confirm the usability of high frequency blocking with the Neuray-II chip electrodes there are still interesting possibilities that could be explored within the sequential stimulation presented as follows.

Considering the work performed on developing the self-running stimulation and impedance test–scripts, described in section 3.7, a development of a script that could run a sequential stimulation could be done in a similar way. This would speed up the stimulation-process by eliminating the manual clicking and also make the process much more consistent.

If this type of stimulation would prove to be successful there are many opportunities opening up for designing advanced patterns in which the electrodes could be activated in a customised order to best block a propagating wave.

5.2 Local effects on the action potential propagation

5.2.1 Evaluation of the analysis method
The functionality of the script developed and the working method for choosing and classifying the cell signal is generally on an acceptable level of accuracy but some details are still to be improved to make the system more consistent.

With the current system, single cell signals have been acquired by studying the fluorescence intensity from the ROIs placed over the cells in the captured time-lapses. The appearance of the single cell signals is very much comparable to the signal acquired for the binned ROIs displayed in Figure 12, section 4.3. The frequently occurring peaks translate as peaks in intracellular calcium which can be correlated to the plateau phase in the action potential where the intracellular calcium is at its highest, this is described in detail in section 2.1.1. It is important to bear in mind when using intracellular calcium levels as an indicator for the

action potential that other processes, that also affect the intracellular calcium level, will come through in the displayed signal. An example of this can be seen in Figure 19 b), section 4.5. Here one can observe the action potential peaks occurring with a frequency of around 0.5 Hz. Before the stimulation, a low frequency process was superimposed on the action potential causing two larger peaks at 10 s and 32 s. The origin of these processes is still not entirely clarified.

In our case, to increase the sample number, we analysed time-lapses with a lowest resolution using a 10x objective, z1.2. Although, this resolution was on the verge for making the placement of ROIs accurate enough to ensure that only the signal from only one cell was gathered by the ROI. Preferably one would use 10x, z2 as the lowest resolution to ensure a more accurate acquisition of signals but since this analysis method was developed after all the experiments were done there was a very limited number of time-lapses to analyse with the higher resolution. Therefore samples with resolution of 10x, z1.2 was decided to be included even if they would introduce some inaccuracy in the single-cell concept.

The choice of parameters to be used for defining distortion, elevation and AF increase was not entirely straight forward. The difficulty was not to define distortion, elevation or AF per se, but rather how to define the parameters so they would not include signals that would pass any of the activation criteria only because of a high noise level. This is the reason for the extra criteria used for exclusion of cells, described in 3.6.2. Also described in this section was that there were some cells that were included in the sample population but not counted as activated cells even if they exhibited parameters that would have let them be counted as an activated cell, according to the script calculations. This exclusion was merely performed on a visual basis where a possible distortion or elevation that was not occurring within a time-frame close to the stimulation was not counted as an activation of the cell. This visual estimation inherently introduces some inaccuracy in which cells that should be included in the sample population or not. A refinement of how to exclude these irregular cells more systematically would preferably be developed, but for that there was unfortunately no time within this study.

Lastly, it is also debatable which accuracy the calculation of the AF is actually providing. There are two main sources of errors within this type of frequency estimation, the sample rate and the peak detection. Concerning the sample rate, the Nyquist criteria states that the highest frequency that can be acquired correctly is the sample rate divided by 2, see equation 2.

$$f_n = \frac{f_s}{2} \qquad\qquad \text{(Eq. 2)}$$

In our experiments, the fastest sampling rate acquired was 0.156 s/frame giving a sampling frequency of 6.41 Hz. According to the Nyquist criteria, the highest frequency that could be reproduced correctly from our time-lapses would thereby be 3.205 Hz. Any signal component that exceeds this frequency can be a source of aliasing that introduces noise into the signal. The most common way to avoid this problem is to sample at a higher rate to ensure that all the frequency components of interest can be detected and the rest of the signal is filtered to avoid the aliasing noise. To increase the sample rate was not an option in our case and the use of a filter was not considered until half-way through the analysis process. Using a filter can also introduce inaccuracy by sorting away high frequency components that are of actual interest for the experiment and therefore we choose to keep on with the analysis by studying the 'raw' unfiltered signal.

The second source of error was the *peakfinder* function used to give an estimation of AF before and after the stimulation by calculating the number of peaks and dividing this number by time elapsed. The function was based on a threshold-solution, where a minimum threshold level in amplitude compared to the surrounding signal level should be met for the peak to be detected. For our script, this threshold was chosen to be kept constant to give the analysis consistency even if it introduced some erroneous detected peaks. Over-all this detection worked fine but for noisy signals and when the signal lost amplitude due to high distortion, the accuracy decreased.

The sampling-rate issue can only be solved by using a faster acquisition system and for this project this was unfortunately not an available option. However, if the intrinsic AF is around 0.7 Hz and the average increase in AF does not result in an AF with the highest value at around 1 Hz as in our experiments, the low sampling rate can be acceptable, see section 4.5. However, to be kept in mind is that these values are achieved with the method discussed above and their accuracy is thereby also debatable.

A solution to the *peakfinder* inaccuracy would be to combine this function with a calculation of the inter-peak-interval (IPI). This is the interval elapsed between two action potential peaks. Hence the peak-detection would still be needed, but an IPI calculation could provide a control to whether the peaks are occurring in a repetitive frequent pattern or not. If the IPI for a series of peaks is very similar,

then the peaks can be classed as a frequent signal. If the IPI on the other hand is largely deviating, the peaks are most certainly due to noise or a very irregular signal, neither of which are wanted for our type of analysis. By introducing this type of calculation a good quality parameter would be given that could indicate if the signal should be used for further analysis or not. Furthermore it would allow a decrease of the amplitude limit that was set up as an exclusion-criterion in section 3.6.2. With the current amplitude limit, most of the noisy signals were excluded but some signals with a clear AF were also excluded on the basis that the signal amplitude was too low. An IPI calculation would here have qualified the clear signal due to a stable IPI value while the noisy signal would have been discarded due to its large IPI deviation.

To conclude, a good foundation for an analysis method for single-cell signal analysis has been developed. The single-cell accuracy can easily be improved by choosing the right magnification and by implementing IPI calculations a higher accuracy could be achieved for signal selection and evaluation. The major draw-back is the limitation of the imaging speed which also limits the resolution for correct frequency detection. However, as with the wave-propagation analysis, this method could be performed in a standard equipped bio-lab which gives it a high usability.

5.2.2   Evaluation of stimulation by pacing-protocols

When there were no obvious changes detected in the propagating action potential waves due to stimulation, the aim was directed towards trying to understand the mechanism action potential propagation on a localised level, in this case including the cell on top of the electrode and its closest neighbours.

The single-cell analyses has enabled extraction of data that can give some indications towards of which events are taking place in the cell at the electrode and in its vicinity. However, as described in section 5.2.1, the analysis method at its current state has some crucial uncertainties to take into account which is why a detailed explanation on the mechanisms on a cellular level will not be given from the data extracted. The analysis was rather focused on the main trends discovered which only can offer a first suggestion of the mechanisms involved. A more specific conclusion cannot be drawn until more accurate data is gathered and also preferably, in a higher sample number.

The very first graph in section 4.3, Figure 13, summarizes the result of this investigation in a good way. Here, one can clearly see that the electrical stimulation did in almost 80% of the trials, were a response was detected,

activate the cell on top of the electrode in some way. The activation was not preserved only for the cell at POS but by looking at the graph in Figure 13 one can detect an almost linearly decreasing percentage of activated cells with an increasing distance to POS. When reaching zone 4 at a distance of 70 μm from POS centre only 20% of the cells are now activated. If the decay in activated cells is truly linear, there would be no activated cells beyond 100 μm from the POS.

5.2.2.1 *The role of gap junctions and the spreading of activation*

One possible explanation to this spread in activation can be offered by the function of gap junctions. As described in section 2.1.3, the gap junctions are tightly coupled ion-channels that enable a direct intercellular transmission of ion-currents. From Claycomb and co-workers we also know that the connexin-43 is present in the HL-1 cells used and this connexin constitutes one of the most common cardiac gap junctions [32, 67, 68]. The ion permeability of the gap junctions is dependent on the connexin that forms the channel. The connexin-43 is however not ion-specific [67].

A possible scenario elicited by the electrical stimulation and explained by the spread of the electrical signal via gap junctions could be stated as follows:

The high amplitude of the electrical stimulation will immediately depolarise the cell at the POS. Since we, with the Fluo-4, are imaging the intracellular calcium the change will be visible as the intracellular calcium reaches its first plateau-level. Since the stimulation causes a strong alternation of the membrane potential, a potential gradient occurs over the gap junctions that connect the cell at POS to its neighbours. The gradient will induce an ion flow through the gap junctions that in turn will alter the membrane potential in the neighbouring cells. If the potential change is high enough, the neighbour might reach its threshold for firing an action potential, see section 2.1.1. In this way, a local electrical stimulation could be carried by ionic currents from the cell at POS to its neighbours and affect them as well.

When studying the fractions of the activation types in Figure 13 one trend is worth a further notice. One can distinguish that activation response by signal elevation or multiple activations, where signal elevation is included, is dominating for cells at POS and is more common for the inner zones than for the outer. Continuing this observation one can see that for the outer zones it is merely an AF increase and distortion that is seen as activation responses.

One possible explanation to this observation could be that, if the cell at POS is not entirely covering the electrode, the stimulation could spread through the medium to the closest neighbouring cells and thereby depolarise them as well. A similar response could probably also be achieved if more than one cell is in direct contact with the electrode. If the signals from these cells would be compared, one would probably not see any difference in the activation times. However, if a situation occurs as displayed in Figure 16, where a delay can be seen between the activation of the cell on POS and the activation of the cells in the other zones, there is a reason to believe that this delay is caused by the transmission of the signal through the gap junctions.

The reason why the elevation is not spread much further than to zone 2 is still debatable. One possible speculation is that the voltage gradient that causes the ion-flow over the gap junctions will decrease with the distance from the POS. The largest voltage gradients will be formed between the cell at the POS and its direct neighbours, the zone 1 cells (Z1c), which would allow a high ion-flow into the Z1c. This ion-flow can elicit an elevation in the intracellular calcium level in the Z1c, but the magnitude will not be the same as for the cell at POS. Since the elevation is lower in the Z1c than at the POS, the gradient formed between the Z1c and its neighbour in zone 2 (Z2c) will therefore not be as strong as between the one in the POS-zone 1 cells, leading to a lower degree of ion flow and thereby lower elevation.

Studying the graph in Figure 16 the delay in the elevation is displayed rather clearly but one can also question if they are actually too slow to be caused by the stimulation. Putting this graph into the context of the normal conduction velocity of cardiac tissue, which is around 50 cm/s, and the conduction velocity over the gap junction itself, 0.1 mm/s [69], one would expect response times within milliseconds and not in several seconds as seen in Figure 16. Important to recall is though that the conduction velocities are relevant for the electrical conduction and displayed in Figure 16 is the intracellular calcium activation. The electrical activation is indeed coupled to the intracellular calcium activation but this activation process can be slower than the actual electrical conduction. Sanderson and co-workers showed that a mechanical elicited elevated calcium level in a single cell caused elevation in intracellular calcium levels among the stimulated cells neighbours by spreading the signal through gap junctions [70]. The activation delay in this response was on the second-scale rather than millisecond which fits better with our graph in Figure 16.

By studying Figure 17 we can achieve some indication of the radial size of the spread of cells activated by electrical stimulation. There was not any big difference between the different frequency-protocols used, all protocols displayed a largest distance to an activated cell at around 70 μm. The numbers in Figure 17 should although be studied with caution. As can be seen in Figure 13, the majority of the outermost activated cells were determined to be activated by an AF increase. As debated in section 5.2.1, the frequency analysis is one of the most vulnerable methods within this analysis, and the accuracy at the current state is somewhat questionable which also makes the longest-distance estimation uncertain.

Before concluding the role of gap junctions for the spreading of our stimulation protocol it is worth mentioning that the age of the culture and its degree of confluency also might be of importance for the spreading of the activation. Our samples were used at 4 or 5 DIV and at this point full confluency was not always reached. If one would have examined the samples at a later stage it is possible that more gap junctions could have been formed and another reach of activation would have been achieved. A possible experiment that could validate whether the spread of activation is carried out by the gap junctions could be by introducing some sort of inhibitor that blocks the gap junctions. Thereby one could also determine the degree of localisation for the stimulation. If all transmission via gap junctions is inhibited, then all cells activated by stimulation are activated directly by the electrode.

To conclude this section, we have registered that not only the cell at the POS but also cells in this vicinity are activated by electrical-pacing stimulation. The spread of this activation seem to be linearly decreasing with distance from the POS and a possible mechanism for the spread can be via a potential shift caused by the intracellular ion-flow allowed by gap junctions. An estimated maximum reach of activation is 70 μm from the centre of POS but to validate this number a more accurate analysis is required.

5.2.2.2   Is pacing possible?
In our experiments, cells experiencing an AF increase of 10 % or larger during electrical stimulation have in this report been classified as paced. However, it might be an unfortunately picked name for the classification.

When returning to the literature on where pacing is performed with the aim of causing arrhythmia or spiral re-entries one realises that during a successful pacing the cellular action potential closely follows the electrical stimulation. This has been demonstrated by Chang and co-workers who displays a captured signal paced by and to 4 Hz [27]. Bian and co-workers could, with their high frequency optical recording system, visualise how their cells could follow a pace even over 5 Hz [24]. Although, all of these studies are performed on cardiac myocytes. Studies on HL-1 cells have used pacing to investigate e.g. its effect on myolysis or conductional changes due to high frequency electrical blocking [28, 29, 25] but actual captions of whether the HL-1 cells follow the pacing stimuli in the same way as cardiac do, were not showed in these cases.

It might be a possibility that the difference between the primary cardiac cells and the HL-1 cells being an immortalised cell line could introduce a difference in ability to be paced. However, as described in section 2.3.2, the HL-1 exhibit many of the important features, especially among the electrophysiological properties, that in many cases makes it comparable to a cardiomyocyte. For this discussion we will therefore assume that the HL-1 have the same ability to be paced as the cardiomyocytes.

With this assumption one would expect to observe higher values in the relatively increased AF for the cells that were stimulated by higher frequency protocols. When studying the comparison of AF increase for different protocols in Figure 18, the result does not follow the expectation. The highest relative AF increase is found with the lowest frequency stimuli protocol, for 1 Hz. The average relative increase for the remaining protocols is around 20 % for all experiments. Nevertheless, once again one has to keep in mind that the AF estimation was one of the analysis methods that still needed some work to improve its accuracy. As explained already in the results section is the large deviation for the 1 Hz protocol is mainly due to one deviating sample and if this sample was removed the relative AF increase for 1 Hz would be more tuned to the level of activation for the 2, 3 and 5 Hz protocols. The deviating sample was nevertheless experiencing a true AF increase which makes it difficult to determine if it should be included in the result or not. The magnitude of this increase was caused by the low AF before stimulation which displayed a limitation with the calculation system. In the future this could to some extent be avoided by introducing a higher limit that the AF must reach for allowing the cell to be included in the analysis.

Even though the sample number in this comparison is not very high, we get with Figure 18 an indication that the pacing might not be working as aimed for since the relative increase of AF is the same for all protocols.

If the improvements in the analysing script and frequency detection were made this could possibly give a more accurate data on the AF deviations. The imaging speed is however still a limitation and the use of calcium imaging will also introduce signal distortion that is not related to the electrical signalling which will remain even if the imaging frame rate is increased.

To give a good validation whether pacing really is occurring with the protocols used, the very best solution would be to aim directly for the source and record the electrical signal with the electrodes present on the chip. Unfortunately, as described in section 2.4.6, a combined recording and stimulation is not possible. However, it is not only the limited line out that is the main issue. Even if more channels were available for multi-site stimulation, there is still one issue remaining due to the large magnitude difference in the stimuli required and the signal to be recorded. As seen in our protocols, amplitudes of up to 1.65 V were applied which were several magnitudes larger than the action potential of around 120 mV. If an electrical stimuli signal is applied in the very near proximity to where electrical recording occurs, the action potential signals would not be detectable beyond the large stimuli signal. One possible solution to this problem is to switch between recording and stimulation at a high frequency. This method has been implemented by Olsson and co-workers but in an *in vivo* probe for neuronal recording [71]. The switching time achieved was 1 ms and the shortest distance between electrode and recording site was 20 μm.

Even though new circuitry technique is rapidly developing, to alter or develop a new chip is time consuming and expensive. If the Neuray-II chip would remain as the primary platform for *in vitro* studies of electrical stimulation at Imec, there are two possible options left from which a validation of the pacing protocols could be performed. The first option is verification with patch clamp measurements, which is briefly described in section 2.4.2. This measurement technique will give a very accurate recording of the intracellular potential, but as mentioned in 2.4.2 the method is very time consuming and can be performed on one to a few cells at a time and can therefore not be used for mapping of the spread of the response. The second option, that would allow mapping, would be to use a voltage-sensitive dye, of which the mechanism was presented in 2.3.3.1. By switching dye, the same imaging process and analysis scripts could still be applied. One could also increase frame-rate by switching to a faster imaging

system, such as an epifluorescent microsocpe. In this way, by capturing membrane voltage-changes instead of intracellular calcium processes it might be possible to obtain a signal response that is more closely following the signal source, the action potential.

To return again to the literature one can ask why e.g Chang and Bian [27, 24] managed to pace the full cell population and we cannot. The answer might be with the electrode and its placement. Both Chang and Bian use a single unipolar electrode that they place on top or at the side of the culture. There are no indications of the electrode size within the papers but estimatied is that the electrodes used are rather on the mm-scale which is far from our µm-sized chip electrodes. The placement of the electrode 'ontop' or 'beside' the cell culture might indicate that neither Chang nor Bian have the same tight seal with the cell as we do. Therefore, when Chang and Bian performed their stimulation they will probably alter the voltage in a larger area then what we did, since the signal will spread through the medium as well. This is merely a speculation but it might also be crucial to why Chang and Bian can perform a full cell population pacing and we cannot. Something that would be interesting to investigate in connection to this reasoning would be multiple site, synchronized stimulation. As mentioned in section 2.4.6, this is not possible with this generation of the chip. Nonetheless, if the line out is improved in the future, a synchronized pacing from several electrodes at once might provide an answer to whether it is a larger stimulated area that is required to reach true pacing.

In conclusion of this section on pacing, we do not yet know if pacing is possible with the Neuray-II chip. The results from our experiments so far show that the relative AF increase is similar for all frequency protocols. For a truly paced cell the relative AF increase would be expected to be higher with increasing pacing frequency. The low temporal resolution of the imaging system and the inaccuracy in the frequency detection makes the achieved results uncertain and further experiments and improved would need to be performed to achieve a valid result. Two options for validation are by using patch clamp and voltage-sensitive dyes. A possible explanation to why pacing is not achieved could be due to the very small area exposed to voltage change by simulation if comparing to other pacing experiments.

5.2.3 Can high frequency stimulation from Neuray-II block the action potential?

Unfortunately there were too few usable time-lapses captured for the high-frequency protocols to make any extensive analysis. However, as seen in

Figure 19, the signal goes from having regularly occurring peaks before stimulation to be distorted and almost completely lacking peaks after the first stimulation for the cell at the POS and one of its neighbours. This response is very similar to what Dura and co-workers achieved when they performed similar experiments [25] and this could be an indication that high frequency blocking could be a possibility with the Neuray-II.

Nonetheless, to be taken into consideration is the fact that the stimulation, as seen in Figure 19, clearly elevates the intracellular calcium but this elevation might mask a signal that is still pulsating. Hence, the intracellular calcium might be very high, which is what is being captured in the signal, but there might be electrical continuous signalling still ongoing but this is not captured with the calcium imaging.

As for the pacing protocols, validating experiments with patch clamp and voltage-sensitive dyes would be of interest to clarify the cellular mechanism due to high frequency stimulation. If further experiments could confirm the high frequency blocking as functional with the Neuray-II chip, an interesting continuation of this experiment would be to implement the sequential stimulation further, as described in 5.1.4.

5.3 Stimulation effect on the Neuray-II chip

To achieve an optimal recording or to perform an efficient stimulation, the impedance of the chip electrode is preferably kept as low as possible. With the chip being exposed to an 'extreme' environment in terms of being soaked in medium which is a solution containing water, different types of ions and many other compounds one could expect that electrochemical reactions might affect the composition of the electrode and thereby also the impedance.

Although, our experiments have so far not showed that stimulation has any sort of influence on the electrode. It is to be noted that the stimulation protocols used for this experiment was adapted from another type of project and the exact stimulation protocols used for pacing or high frequency blocking were not tested.

Nonetheless, for the protocols tested there was no difference in impedance for electrodes used for stimulation and for those measured as controls, as have been exemplified with Figure 21.

The only change that did occur, displayed in Figure 22, was a small increase in impedance after the over-night stimulation. The degree of change was equal for stimulated and non stimulated electrodes which gave an indication that ageing rather was the reason for the impedance increase. This aging behaviour has been confirmed by other in-house experiments which have resulted in a current maximal use of chips to 2 weeks in culture.

6 Conclusions and future perspectives

With this project, the possibilities of using the Neuray-II chip, developed at Imec, as a platform for studies of cardiac pacing and arrhythmia have been explored.

The cell-line, HL-1, which was chosen to provide the target cells for this *in vitro-* model was well compatible with the chip and displayed spontaneously occurring calcium waves after 4-5 DIV and occasionally re-entrant spirals. The cellular action potentials were visualised with calcium imaging and the fluorescent signals were captured in time-lapses during the stimulation-experiments.

A few attempts were done to pattern glass cover-slips and chips with micro-contact printing and silicone inserts to introduce a structure in the cell culture which would affect the action potential propagation. These experiments were not very successful, mostly due to difficulties of inducing a pattern on the same scale as the cellular network. The pattern induced by the stamp was too small to make a change in cell growth and the silicone insert was too big and left too few cells to remain on the chip after taking it off. Improvements of both techniques could be done but was not prioritised within this project and focus was rather put on the electrical stimulation.

On a macroscopic level, no large overall change in the propagation of action potentials waves could be detected due to local electrical stimulation. Neither was any induction or termination of re-entrant spirals to be seen from either pacing protocols or from high frequency protocols. This led to the conclusion that an eventual response from localised electrical stimulation is limited in its spread within the cellular population, which also set the aim for further investigation.

However, to enable the initial macroscopic analysis of the time-lapses, a Matlab-script displaying the propagation of the action potential waves was developed. The script could successfully recreate the gathered signal into sequential timeslots displaying matrix-plots of the propagation delay of the action potential waves. The analysis methods main limitation was the low temporal resolution of the imaging which restricted the usage of the script to time-lapses acquired by using 10x objective, z0.7 or lower resolutions. Nevertheless, if the imaging frame-rate could be increased alongside with two script adjustments to improve the accuracy and readability, the analysis method could be very promising. The main strengths of the analysis technique are (i) high spatial resolution compared

to similar methods, (ii) high usability – only standard lab equipment is needed, (iii) no sample transparency required, which is crucial when imaging cell cultures on a chip, (iv) versatility – the script could be used on other types of fluorescent dyes such as voltage-sensitive dyes.

To investigate the local effect of stimulation, a second analysis method, including development of a Matlab-script was performed. The script allowed the user to analyse the signals from systematically chosen single cells and evaluate the response to stimulation in terms of elevation of signal base-level, distortion in amplitude and frequency change. The script makes a good foundation for single-cell signal analysis but needs further development of the frequency-detection to become more accurate. As for the propagation-delay plots, this analysis also suffered from the low temporal resolution in the imaging and to achieve fully functional frequency detection an increased frame-rate is a requirement.

The results from the single-cell analysis where pacing protocols were used for stimulation indicated that the stimulation applied only causes a local change of the action potentials in the culture. For the cultures analysed, 4-5 DIV, the maximum spread in cell activation due to stimulation was 70 μm from the POS. The number of cells that was activated decreased with increased distance to the POS and the strongest signal response, e.g. high elevation of signal base-level, was observed close to the POS. A possible explanation to the spread of the activation is that the electrical change is transmitted through the gap junctions that connect the cells to each other. The indications of this very local spread could be the explanation to why no drastic changes could be seen in the macroscopic investigation.

There were a very limited number of samples to be used for single-cell analysis and they were not always of the best quality in terms of resolution and cell quality, which is why the results only should be looked at as indications. To verify the results, the Matlab-script should be improved, sample number should be increased and captions should have high enough resolution to ensure that signal from individual cells are captured. To investigate the gap junction spreading theory, stimulation experiments could be performed in a culture where gap junctions are inhibited by a blocking agent.

The frequency analysis of the stimulated cell does not give any indication that true pacing is reached since the relative AF increase was the same for all tested pacing protocols. However, the results achieved from the current analysis

method are too uncertain to draw any relevant conclusions from. As mentioned above, a higher temporal resolution for the imaging is necessary to provide a signal with the accuracy needed for analysis and script improvements are needed improve the frequency detection. After these improvements conclusions can be drawn, preferably with verifying experiments from patch clamp and with voltage-sensitive dyes.

The single-cell analysis on cells stimulated with high frequency protocols indicated that a block of the action potential might be possible. Although, a higher sample number is required for accuracy and, verification with patch clamp and mapping with voltage-sensitive dye would be of interest. If high frequency blocking by electrical stimulation would prove to be possible, further implementation of a systematic sequential stimulation would be of high interest since it might enable blocking of propagating waves or spirals.

As a system-verification, the effect of electrical stimulation on electrode impedance was also performed. The impedance experiments did not however show any difference in impedance between used and non-used electrodes and no restrictions needs to be taken into consideration regarding stimulation. Although, it has been showed that aging is of importance for the electrode impedance and usage is restricted to 2 weeks.

To summarise these conclusions we can see that the Neuray-II chip is a safe-to-use stimulating system which is at its current state limited in its usage to 2 weeks in culture which is acceptable for cardiac and HL-1 cultures. The system offers mainly a very localised electrical stimulation by which it has until today not yet proven to be possible to cause macroscopic changes, such as altering action potential propagation, or to induce or terminate re-entrant spirals. We have nevertheless developed in this project the foundation of tools to analyse the action potential propagation both on a macroscopic and on a cellular level. With these tools we have also reached one step further in our understanding of the effect of the cellular response due to electrical stimulation and its spreading on a local level. With improved tools, a more accurate analysis of the cellular response and its local effect it might be possible to use the knowledge gathered to implement more advanced stimulation patterns involving several electrodes such as sequential stimulation and thereby cause a macroscopic effect.

In conclusion we can state that the Neuray-II chip as it currently stands would not be able to serve as good platform as an *in vitro* model for cardiac pacing and arrhythmia. With this project we have created the foundation of the tools needed

for the analysis and received the basic knowledge required, both within cellular response and technical possibilities and limitations, to enable the development of a functional *in vitro* study model.

7 References

[1] T. Laske, A. Dopp, and P. Iaizzo, "Pacing and defibrillation," in *Handbook of Cardiac Anatomy, Physiology, and Devices*, P. A. Iaizzo, Ed. Humana Press, 2009, pp. 443–473. [Online]. Available: http://dx.doi.org/10.1007/978-1-60327-372-5_27

[2] M. Nichols, N. Townsend, R. Luengo-Fernandez, J. Leal, A. Gray, P. Scarborough, and R. M, "European cardiovascular disease statistics 2012," 2012.

[3] D. Braeken, "Bioelectronic interfacing: Electrical and chemical sensing of biological signals," Ph.D. dissertation, 2009.

[4] S. Nattel, "New ideas about atrial fibrillation 50 years on," *Nature*, vol. 415, no. 6868, pp. 219–226, 2002.

[5] D. M. Bers, "Cardiac excitation–contraction coupling," *Nature*, vol. 415, no. 6868, pp. 198–205, 2002.

[6] C.-h. Luo and Y. Rudy, "A model of the ventricular cardiac action potential. depolarization, repolarization, and their interaction." *Circulation research*, vol. 68, no. 6, pp. 1501–1526, 1991.

[7] V. Barnett, "Cellular myocytes," in *Handbook of Cardiac Anatomy, Physiology, and Devices*, P. A. Iaizzo, Ed. Humana Press, 2009, pp. 147–158. [Online]. Available: http://-dx.doi.org/10.1007/978-1-60327-372-5_10

[8] M. Baruscotti, A. Bucchi, and D. DiFrancesco, "Physiology and pharmacology of the cardiac pacemaker ("funny") current," *Pharmacology & therapeutics*, vol. 107, no. 1, pp. 59–79, 2005.

[9] D. DiFrancesco, "The role of the funny current in pacemaker activity," *Circulation research*, vol. 106, no. 3, pp. 434–446, 2010.

[10] D. DiFrancesco, "Pacemaker mechanisms in cardiac tissue," *Annual review of physiology*, vol. 55, no. 1, pp. 455–472, 1993.

[11] H. Yu, F. Chang, and I. S. Cohen, "Pacemaker current i (f) in adult canine cardiac ventricular myocytes." *The Journal of physiology*, vol. 485, no. Pt 2, pp. 469–483, 1995.

[12] S. Kanno, J. E. Saffitz *et al.*, "The role of myocardial gap junctions in electrical conduction and arrhythmogenesis," *Cardiovascular Pathology*, vol. 10, no. 4, pp. 169–178, 2001.

[13] T. Laske, M. Shrivastav, and P. Iaizzo, "The cardiac conduction system," in *Handbook of Cardiac Anatomy, Physiology, and Devices*, P. A. Iaizzo, Ed. Humana Press, 2009, pp. 159–175. [Online]. Available: http://dx.doi.org/10.1007/978-1-60327-372-5_11

[14] I. Cohen and R. Robinson, "Pacemaker current and automatic rhythms: Toward a molecular understanding," in *Basis and Treatment of Cardiac Arrhythmias*, ser. Handbook of Experimental Pharmacology. Springer Berlin Heidelberg, 2006, vol. 171, pp. 41–71. [Online]. Available: http://dx.doi.org/10.1007/3-540-29715-4_2

[15] M. Janse and M. Rosen, "History of arrhythmias," in *Basis and Treatment of Cardiac Arrhythmias*, ser. Handbook of Experimental Pharmacology. Springer Berlin Heidelberg, 2006, vol. 171, pp. 1–39. [Online]. Available: http://dx.doi.org/10.1007/3-540-29715-4_1

[16] B. F. Hoffman and M. R. Rosen, "Cellular mechanisms for cardiac arrhythmias." *Circulation research*, vol. 49, no. 1, pp. 1–15, 1981.

[17] M. A. Allessie, F. Bonke, and F. Schopman, "Circus movement in rabbit atrial muscle as a mechanism of tachycardia. iii. the" leading circle" concept: a new model of circus movement in cardiac tissue without the involvement of an anatomical obstacle." *Circulation Research*, vol. 41, no. 1, p. 9, 1977.

[18] J. J. Lee, K. Kamjoo, D. Hough, C. Hwang, W. Fan, M. C. Fishbein, C. Bonometti, T. Ikeda, H. S. Karagueuzian, and P.-S. Chen, "Reentrant wave fronts in wiggers' stage ii ventricular fibrillation characteristics and mechanisms of termination and spontaneous regeneration," *Circulation research*, vol. 78, no. 4, pp. 660–675, 1996.

[19] K. Konings, C. Kirchhof, J. Smeets, H. Wellens, O. C. Penn, and M. A. Allessie, "High-density mapping of electrically induced atrial fibrillation in humans," *Circulation*, vol. 89, no. 4, pp. 1665–1680, 1994.

[20] T. Y. Kim, S.-J. Woo, S.-m. Hwang, J. H. Hong, and K. J. Lee, "Cardiac beat-to-beat alternations driven by unusual spiral waves," *Proceedings of the National Academy of Sciences*, vol. 104, no. 28, pp. 11639–11642, 2007.

[21] J. H. Hong, J. H. Choi, T. Y. Kim, and K. J. Lee, "Spiral reentry waves in confluent layer of hl-1 cardiomyocyte cell lines," *Biochemical and biophysical research communications*, vol. 377, no. 4, pp. 1269–1273, 2008.

[22] S.-m. Hwang, K.-h. Yea, and K. J. Lee, "Regular and alternant spiral waves of contractile motion on rat ventricle cell cultures," *Phys. Rev. Lett.*, vol. 92, p. 198103, May 2004. [Online]. Available: http://link.aps.org/doi/10.1103/PhysRevLett.92.198103

[23] W. A. Tacker and L. A. Geddes, "The laws of electrical stimulation of cardiac tissue," *Proceedings of the IEEE*, vol. 84, no. 3, pp. 355–365, 1996.

[24] W. Bian and L. Tung, "Structure-related initiation of reentry by rapid pacing in monolayers of cardiac cells," *Circulation research*, vol. 98, no. 4, pp. e29–e38, 2006.

[25] B. Dura, G. T. Kovacs, and L. Giovangrandi, "Spatiotemporally controlled cardiac conduction block using high-frequency electrical stimulation," *PloS one*, vol. 7, no. 4, p. e36217, 2012.

[26] D.-H. Kim, E. A. Lipke, P. Kim, R. Cheong, S. Thompson, M. Delannoy, K.-Y. Suh, L. Tung, and A. Levchenko, "Nanoscale cues regulate the structure and function of macroscopic cardiac tissue constructs," *Proceedings of the National Academy of Sciences*, vol. 107, no. 2, pp. 565–570, 2010.

[27] M. G. Chang, Y. Zhang, C. Y. Chang, L. Xu, R. Emokpae, L. Tung, E. Marbán, and M. R. Abraham, "Spiral waves and reentry dynamics in an in vitro model of the healed infarct border zone," *Circulation research*, vol. 105, no. 11, pp. 1062–1071, 2009.

[28] B. J. Brundel, H. H. Kampinga, and R. H. Henning, "Calpain inhibition prevents pacing-induced cellular remodeling in a hl-1 myocyte model for atrial fibrillation," *Cardiovascular research*, vol. 62, no. 3, pp. 521–528, 2004.

[29] B. J. Brundel, A. Shiroshita-Takeshita, X. Qi, Y.-H. Yeh, D. Chartier, I. C. van Gelder, R. H. Henning, H. H. Kampinga, and S. Nattel, "Induction of heat shock response protects the heart against atrial fibrillation," *Circulation research*, vol. 99, no. 12, pp. 1394–1402, 2006.

[30] S. Iravanian, Y. Nabutovsky, C.-R. Kong, S. Saha, N. Bursac, and L. Tung, "Functional reentry in cultured monolayers of neonatal rat cardiac cells," *American Journal of Physiology-Heart and Circulatory Physiology*, vol. 285, no. 1, pp. H449–H456, 2003.

[31] Z. Y. Lim, B. Maskara, F. Aguel, R. Emokpae Jr, and L. Tung, "Spiral wave attachment to millimeter-sized obstacles," *Circulation*, vol. 114, no. 20, pp. 2113–2121, 2006.

[32] W. C. Claycomb, N. A. Lanson, B. S. Stallworth, D. B. Egeland, J. B. Delcarpio, A. Bahinski, and N. J. Izzo, "Hl-1 cells: a cardiac muscle cell line that contracts and retains phenotypic characteristics of the adult cardiomyocyte," *Proceedings of the National Academy of Sciences*, vol. 95, no. 6, pp. 2979–2984, 1998.

[33] S. M. White, P. E. Constantin, and W. C. Claycomb, "Cardiac physiology at the cellular level: use of cultured hl-1 cardiomyocytes for studies of cardiac muscle cell structure and function," *American Journal of Physiology-Heart and Circulatory Physiology*, vol. 286, no. 3, pp. H823–H829, 2004.

[34] L. Sartiani, P. Bochet, E. Cerbai, A. Mugelli, and R. Fischmeister, "Functional expression of the hyperpolarization-activated, non-selective cation current if in immortalized hl-1 cardiomyocytes," *The Journal of physiology*, vol. 545, no. 1, pp. 81–92, 2002.

[35] L. M. Loew, "Potentiometric dyes: Imaging electrical activity of cell membranes," *Pure & Applied Chemistry*, vol. 68, no. 7, pp. 1405–1409, 1996.

[36] I. R. Efimov, V. P. Nikolski, and G. Salama, "Optical imaging of the heart," *Circulation research*, vol. 95, no. 1, pp. 21–33, 2004.

[37] B. Baker, E. Kosmidis, D. Vucinic, C. Falk, L. Cohen, M. Djurisic, and D. Zecevic, "Imaging brain activity with voltage- and calcium-sensitive dyes," *Cellular and Molecular Neurobiology*, vol. 25, no. 2, pp. 245–282, 2005. [Online]. Available: http://dx.doi.org/-10.1007/s10571-005-3059-6

[38] P. Schaffer, H. Ahammer, W. Müller, B. Koidl, and H. Windisch, "Di-4-anepps causes photodynamic damage to isolated cardiomyocytes," *Pflügers Archiv*, vol. 426, no. 6, pp. 548–551, 1994.

[39] A. P. Larsen, K. J. Sciuto, A. P. Moreno, and S. Poelzing, "The voltage-sensitive dye di-4-anepps slows conduction velocity in isolated guinea pig hearts," *Heart Rhythm*, 2012.

[40] K. R. Gee, K. Brown, W. Chen, J. Bishop-Stewart, D. Gray, and I. Johnson, "Chemical and physiological characterization of fluo-4 ca (2+)-indicator dyes." *Cell calcium*, vol. 27, no. 2, p. 97, 2000.

[41] A. Minta, J. Kao, and R. Y. Tsien, "Fluorescent indicators for cytosolic calcium based on rhodamine and fluorescein chromophores." *Journal of Biological Chemistry*, vol. 264, no. 14, pp. 8171–8178, 1989.

[42] O. H. Petersen, *Measuring calcium and calmodulin inside and outside cells*. Springer Verlag, 2001.

[43] A. Grinvald, R. Frostig, E. Lieke, and R. Hildesheim, "Optical imaging of neuronal activity." *Physiological reviews*, vol. 68, no. 4, pp. 1285–1366, 1988.

[44] J. B. Pawley, *Handbook of biological confocal microscopy*. Springerverlag Us, 2006.

[45] L. Tung and Y. Zhang, "Optical imaging of arrhythmias in tissue culture," *Journal of electrocardiology*, vol. 39, no. 4, pp. S2–S6, 2006.

[46] V. Sharma, R. C. Susil, and L. Tung, "Paradoxical loss of excitation with high intensity pulses during electric field stimulation of single cardiac cells," *Biophysical journal*, vol. 88, no. 4, pp. 3038–3049, 2005.

[47] A. Hierlemann, U. Frey, S. Hafizovic, and F. Heer, "Growing cells atop microelectronic chips: Interfacing electrogenic cells in vitro with cmos-based microelectrode arrays," *Proceedings of the IEEE*, vol. 99, no. 2, pp. 252–284, 2011.

[48] A. Molleman, *Basic Theoretical Principles*. John Wiley & Sons, Ltd, 2003, pp. 5–42. [Online]. Available: http://dx.doi.org/10.1002/0470856521.ch2

[49] S. Szunerits and L. Thouin, "10 - microelectrode arrays," in *Handbook of Electrochemistry*, C. G. Zoski, Ed. Amsterdam: Elsevier, 2007, pp. 391 – XI. [Online]. Available: http://-www.sciencedirect.com/science/article/pii/B9780444519580500239

[50] A. L. Hodgkin and A. F. Huxley, "A quantitative description of membrane current and its application to conduction and excitation in nerve," *The Journal of physiology*, vol. 117, no. 4, p. 500, 1952.

[51] R. Huys, "Cmos microelectrode arrays for neurophysiological applications (cmos micro-electrode arrays voor neurofysiologische toepassingen)," Ph.D. dissertation, 2011.

[52] S. F. Cogan, "Neural stimulation and recording electrodes," *Annu. Rev. Biomed. Eng.*, vol. 10, pp. 275–309, 2008.

[53] J. O. Bockris, A. K. Reddy, and M. E. Gamboa-Adelco, "The electrified interface," in *Modern Electrochemistry 2A*. Springer US, 2002, pp. 771–1033. [Online]. Available: http://-dx.doi.org/10.1007/0-306-47605-3_1

[54] W. Baumann, M. Lehmann, A. Schwinde, R. Ehret, M. Brischwein, and B. Wolf, "Microelectronic sensor system for microphysiological application on living cells," *Sensors and Actuators B: Chemical*, vol. 55, no. 1, pp. 77–89, 1999.

[55] R. Ehret, W. Baumann, M. Brischwein, M. Lehmann, T. Henning, I. Freund, S. Drechsler, U. Friedrich, M.-L. Hubert, E. Motrescu *et al.*, "Multiparametric microsensor chips for screening applications," *Fresenius' journal of analytical chemistry*, vol. 369, no. 1, pp. 30–35, 2001.

[56] M. Brischwein, E. Motrescu, E. Cabala, A. Otto, H. Grothe, and B. Wolf, "Functional cellular assays with multiparametric silicon sensor chips," *Lab on a Chip*, vol. 3, no. 4, pp. 234–240, 2003.

[57] P. Wang, G. Xu, L. Qin, Y. Xu, Y. Li, and R. Li, "Cell-based biosensors and its application in biomedicine," *Sensors and Actuators B: Chemical*, vol. 108, no. 1, pp. 576–584, 2005.

[58] R. K. Clark, *Anatomy and physiology: Understanding the human body*. Jones & Bartlett Pub, 2005.

[59] M. E. Spira and A. Hai, "Multi-electrode array technologies for neuroscience and cardiology," *Nature nanotechnology*, vol. 8, no. 2, pp. 83–94, 2013.

[60] R. Huys, D. Braeken, D. Jans, A. Stassen, N. Collaert, J. Wouters, J. Loo, S. Severi, F. Vleugels, G. Callewaert *et al.*, "Single-cell recording and stimulation with a 16k micro-nail electrode array integrated on a 0.18 μm cmos chip," *Lab on a Chip*, vol. 12, no. 7, pp. 1274–1280, 2012.

[61] D. Braeken, R. Huys, J. Loo, C. Bartic, G. Borghs, G. Callewaert, and W. Eberle, "Localized electrical stimulation of in vitro neurons using an array of sub-cellular sized electrodes," *Biosensors and Bioelectronics*, vol. 26, no. 4, pp. 1474–1477, 2010.

[62] D. Braeken, D. Jans, R. Huys, A. Stassen, N. Collaert, L. Hoffman, W. Eberle, P. Peumans, and G. Callewaert, "Open-cell recording of action potentials using active electrode arrays," *Lab Chip*, vol. 12, pp. 4397–4402, 2012. [Online]. Available: http://dx.doi.org/10.1039/-C2LC40656J

[63] C. Xie, Z. Lin, L. Hanson, Y. Cui, and B. Cui, "Intracellular recording of action potentials by nanopillar electroporation," *Nature nanotechnology*, vol. 7, no. 3, pp. 185–190, 2012.

[64] S. P. Carey, J. M. Charest, and C. A. Reinhart-King, "Forces during cell adhesion and spreading: implications for cellular homeostasis," in *Cellular and Biomolecular Mechanics and Mechanobiology*. Springer, 2011, pp. 29–69.

[65] J. Vienken, U. Zimmermann, M. Fouchard, and D. Zagury, "Electrofusion of myeloma cells on the single cell level: Fusion under sterile conditions without proteolytic enzyme treatment," *FEBS letters*, vol. 163, no. 1, pp. 54–56, 1983.

[66] W. Chen and R. C. Lee, "An improved double vaseline gap voltage clamp to study electroporated skeletal muscle fibers," *Biophysical journal*, vol. 66, no. 3, pp. 700–709, 1994.

[67] S. Dhein, *Cardiac Gap Junctions: Physiology, Regulation, Pathophysiology, and Pharmacology*. Karger Publishers, 1998.

[68] W. H. Evans and P. E. Martin, "Gap junctions: structure and function (review)," *Molecular membrane biology*, vol. 19, no. 2, pp. 121–136, 2002.

[69] S. Rohr, "Role of gap junctions in the propagation of the cardiac action potential," *Cardiovascular research*, vol. 62, no. 2, pp. 309–322, 2004.

[70] M. J. Sanderson, A. C. Charles, S. Boitano, and E. R. Dirksen, "Mechanisms and function of intercellular calcium signaling," *Molecular and cellular endocrinology*, vol. 98, no. 2, pp. 173–187, 1994.

[71] R. H. Olsson III, D. L. Buhl, A. M. Sirota, G. Buzsaki, and K. D. Wise, "Band-tunable and multiplexed integrated circuits for simultaneous recording and stimulation with microelectrode arrays," *Biomedical Engineering, IEEE Transactions on*, vol. 52, no. 7, pp. 1303–1311, 2005.